UNIVERSITY OF CALIFORNIA
RIVERSIDE

Computational Assessment of Liquids That Capture Carbon Through Physisorption

A Thesis submitted in partial satisfaction
of the requirements for the degree of

Master of Science

in

Chemistry

by

Nicole Christine Onishi Feider

June 2021

Thesis Committee:
Dr. De-en Jiang, Chairperson
Dr. Gregory Beran
Dr. Yadong Yin

The Thesis of Nicole Christine Onishi Feider is approved:

_____

_____

_____

Committee Chairperson

University of California, Riverside

ACKNOWLEDGMENT OF COPYRIGHT

The text and figures in Chapter 2 are reproduced from Journal of Molecular Liquids, Vol. 335, Nicole Onishi Feider, Shannon M. Mahurin, Chi-Linh Do-Thanh, Sheng Dai, and De-en Jiang, Molecular dynamics simulations of a dicationic ionic liquid for CO_2 capture, 116163, 2021, DOI: 10.1016/j.molliq.2021.116163, with permission from Elsevier.

ACKNOWLEDGMENTS

There are so many people who contributed to my success, in all ways, big and small, that it would be impossible to name them all. I feel extremely lucky to have been given the opportunities I have, and to have met such amazing people along the way.

First, I'd like to thank my PI, Dr. De-en Jiang, for his support and guidance as a mentor to me in this journey. Thank you to my fellow labmates for their kindness and troubleshooting help, to my friends and family for pretending to be interested in my research, and to my students, as teaching them was truly the most joyous part of graduate school. I also want to thank the professors and staff who inspired and encouraged me, both at the University of California, Riverside, and at Western Washington University.

Thank you to my lovely cat, Günder, for snuggles through the good and the bad. Above all, a special thank you to my husband, Colton, for everything, for believing in me when I did not myself, and sticking by my side through it all.

ABSTRACT OF THE THESIS

Computational Assessment of Liquids That Capture Carbon Through Physisorption

by

Nicole Christine Onishi Feider

Master of Science, Graduate Program in Chemistry
University of California, Riverside, June 2021
Dr. De-en Jiang, Chairperson

Carbon capture and gas separation is of great importance in addressing climate change, as greenhouse gas emissions continue to rise with major contributions from transportation and electricity production. Some materials have shown great affinity for CO_2 capture, like metal-organic frameworks, zeolites, and functionalized ionic liquids. Limitations in these materials, such as regeneration costs, make it advantageous to develop porous media that are liquids at room temperature. This work employs computational chemistry to study two liquids used for gas separations: an ionic liquid with a polyethylene glycol-linked dication, and a novel porous ionic liquid with a permanent pore large enough to house small gas molecules. Using classical molecular dynamics, we are able to understand the behavior of these liquids on the atomic level, and design new materials to effectively tune their properties.

The dicationic ionic liquid, [DBU-PEG][Tf_2N]$_2$, was synthesized previously, though not studied computationally. We find that our model well-replicated experimentally determined density, viscosity, and powder x-ray diffraction spectra. Our

work reveals that the geminal dication, connecting two bicyclic amidine groups with a polyethylene glycol linker, plays a unique role in CO_2 absorption, resulting from both the dication's shape and charge distribution. We also present an anionic covalent cage-based porous liquid—the cage featuring a 4.25 Å pore. We simulate the bulk liquid with CO_2, CH_4, and N_2 molecules, and find a strong preference for CO_2 capture from the gas-cage interactions. This is supported by analysis of a gas molecule's time-of-stay inside a cage, diffusivity of the gases in the system, and predicted solubilities from grand canonical Monte Carlo methods. The liquid also presents energetic and thermodynamic favorability for CO_2 over the other gases studied.

This work investigates two unique liquids' performances in capturing carbon, and encourages further development of tunable liquids for gas separations. The geminal design of the cation in [DBU-PEG][Tf_2N]$_2$ inspires a similar approach of using dianions in ionic liquids, while the modular synthesis of the porous liquid can be easily modified to feature other functional groups. Such changes may lead to considerable effects in gas uptake and selectivity, and should be studied further.

Table of Contents

List of Figures

List of Tables

CHAPTER ONE

Introduction

1.1 Overview

This thesis focuses on the computational study of liquids used for the purpose of separations, particularly in carbon capture methods, and primarily employing classical molecular dynamics (CMD) simulations. The systems presented in this work have been synthesized and studied experimentally, but future simulation may prove useful in tuning and designing novel materials similar to those shown here. Chapter 1 introduces the present state of the field of liquids for gas separations, such as ionic liquids (ILs) and porous liquids (PLs), as well as how computational methods have been used to study them. Chapter 2 is centered on the IL [DBU-PEG][Tf_2N]$_2$, which is designed to enhance carbon dioxide (CO_2) interactions with a unique dication, hosting a polyethylene glycol (PEG) linker. Chapter 3 changes focus to a cage-based PL with permanent pores large enough to contain 1 to 3 small gas molecules. Chapter 4 concludes and summarizes the work herein, and discusses future directions for the field.

1.2 Materials for gas separations

In a Nature comment article, seven chemical separations are featured, which "if improved, would reap great global benefits".[1] Among these seven is greenhouse gas separation. With temperatures continuing to rise due to climate change, the need for more sustainable and efficient methods of combating greenhouse gas emissions is of great

importance. The separations of primary interest are CO_2 from gas mixtures also containing methane (CH_4) or nitrogen gas (N_2).[1] One method uses aqueous amines for CO_2 scrubbing, and while relatively cheap and effective in chemically binding CO_2 to the amine, there are a variety of issues with this method.[2] These solvents tend to degrade over time, are corrosive, and with a high vapor pressure, evaporate easily.[2] Along with that, the chemisorption of CO_2 to the amine requires a high energetic input to regenerate the solvent.[2]

One way to address this issue is done by employing physisorption, which has a lower energetic barrier than chemisorption, and therefore makes for a less costly alternative. Porous materials generally achieve carbon capture through physisorption, and have been studied as a means of gas separation. Common porous materials include activated carbon, metal organic frameworks (MOFs), and zeolites.[3,4] They may range in pore size and shape, chemical makeup, and serve a variety of applications not limited to separations. Frameworks which have organic linking groups, like covalent organic frameworks (COFs) and MOFs, may be designed with an endless variety of linking groups.[5,6] Such versatility is attractive for those wanting to tune very precisely the size and shape of the pores in a material, potentially therefore tuning selectivity of gas separations. One drawback is that the materials listed before exist in the solid state at room temperature. Electricity production is a large contributor to greenhouse gas emissions, and for such large scale operations, gas separation media that can be applied to a flow process is more desirable. This of course is more difficult with solids rather than liquids, thus driving the exploration of liquid gas separation media.

1.3 Ionic liquids for carbon capture

ILs, which boast a low vapor pressure and chemical tunability, have been studied for CO_2 capture as bulk liquids used in flow processes, within supported ionic liquid membranes (SILMs), and as solvents in PLs.[7-9] Conventional ILs perform carbon capture through physisorption, and have a CO_2 absorption enthalpy of about -20 kJ/mol.[10] In these ILs, absorption is largely reliant on the anions used, though the cation does play some minor role. On the other hand, the enthalpy of CO_2 absorption of functionalized ILs, which absorb CO_2 through chemisorption, is roughly -80 kJ/mol.[10] Compared to functionalized ILs, conventional ILs tend to have a lower CO_2 absorption capacity, because the interaction between CO_2 and the IL is weaker, however the cost of regeneration is lessened.

ILs present their own challenges versus other separation media, such as high viscosity which generally increases further with CO_2 absorption. Additionally, balancing between higher uptake and lower regeneration costs is a point of interest in improving ILs for carbon capture. However, the nonvolatility of ILs makes for a less energy-consumptive and environmentally costly option compared to other separation methods like amine scrubbing, mentioned earlier. The ability to implement various functional groups on both the anion and the cation has allowed for vast improvements of these materials, minimizing the viscosity change and tuning the enthalpy of CO_2 binding.[10-12]

1.4 Porous liquids

PLs were first introduced by O'Reilly et al as a concept in 2007, described as liquids which have intrinsic porosity.[13] In a way, traditional liquids do have pores, that is the empty space *between* molecules, but those cavities are irregular, transient, and impermanent. This is coined as extrinsic porosity, and in contrast, intrinsic porosity requires "permanent, empty, well-defined cavities *within* molecules of the liquid, or in particles dispersed within it".[13] Three classes of PLs were proposed, illustrated in Figure 1.1. Type 1 PLs are neat liquids with intrinsic porosity, as in, they do not require additional solvents to behave as a liquid at room temperature. Type 2 PLs are composed of porous molecules which are dissolved into a solvent to achieve fluidity. These usually involve bulky solvents, like crown ethers, to ensure that the cavity remains empty upon dissolution. Type 3 PLs are similar to Type 2, except they feature a framework dispersed in a solvent that, again, does not interfere with the porosity.

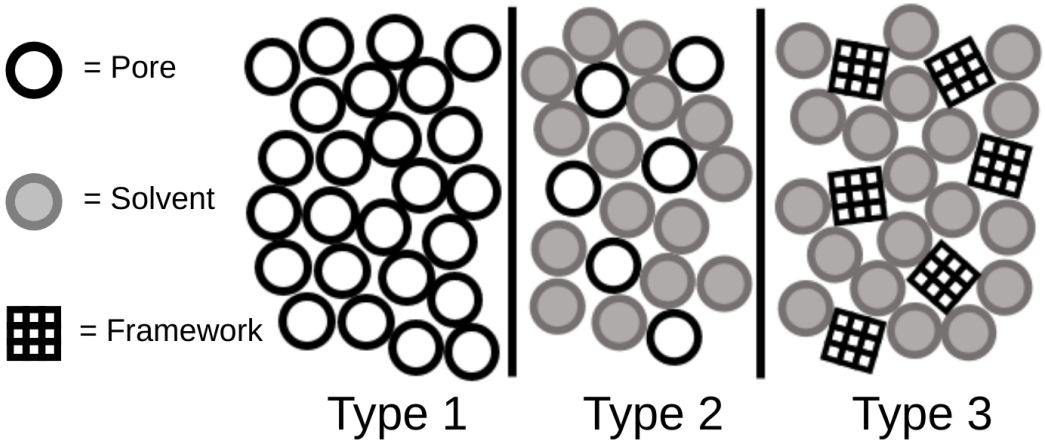

Figure 1.1 Cartoon depiction of types 1, 2, and 3 porous liquids.

Porous organic cages (POCs) synthesized through amine condensation were an early candidate for future PLs.[14-16] Their simple synthesis through small building blocks make the addition of various functional groups easy, and the reactants could be swapped out to adjust the size and shape of the POC. A cage resulting from a stoichiometric ratio of six ethylenediamine and four 1,3,5-benzenetricarboxaldehyde, as drawn in Figure 1.2, resembles a truncated tetrahedron with four windows, contains a cavity about 5 Å in diameter, and is fairly rigid, limiting the risk of collapse and loss of porosity. One of the first attempts in transforming this POC to a PL was done by adding long alkyl chains to the ethylenediamine groups to lower the melting point of the POC, proposing a Type 1 PL.[16] While this did result in a liquid at room temperature, the alkyl chains were thin enough to enter the pores of nearby cages, thus creating a non-porous liquid. Eventually, the same group was successful in synthesizing a Type 2 microporous liquid with the same POC backbone, attaching oligoether loops to the ethylenediamines and dissolving in 15-crown-5 ether.[17]

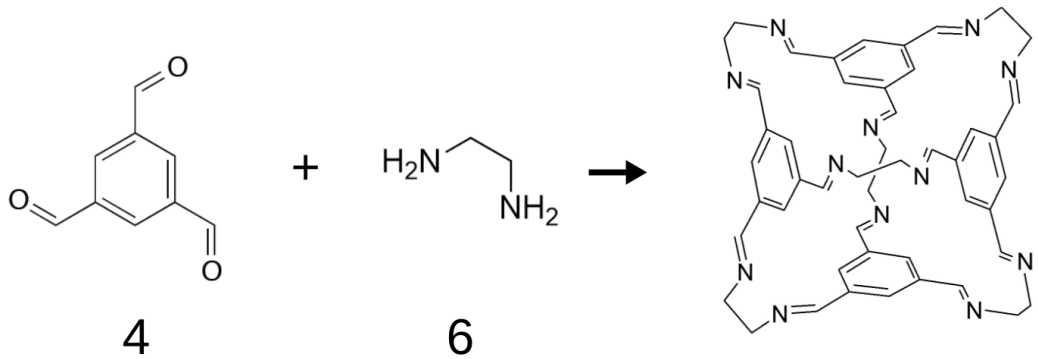

Figure 1.2 Synthesis of tetrahedral cage via imine formation reaction.

While much of the literature surrounding PLs features Type 3 and cage-based liquids, there have been a few PLs reported that get their porosity through other structures. One notable case, a porous ionic liquid (PIL) from Zhang et al, has a corona design, attaching organosilane groups to the surface of a hollow silica sphere, and pairing with a PEG-based counterion.[18] The hollow spheres (HSs) are about 14 nm in diameter, giving this Type 1 PL mesoporosity. The same empty host, dissolved in an ionic liquid, showed higher solubility of CO_2 than N_2, suggesting that it may be used for CO_2/N_2 separations.[19] There has also been some discussion on the use of cyclodextrins (CDs) in PLs, as their ring shape provides a small central cavity, and polymer networks containing CD analogs had some porosity.[13,20,21] The empty spaces in these polymers, however, were more likely due to the cavities between different CDs rather than those within a single CD.[21] The backbone of the CD is also quite flexible, increasing the chance of collapse.[13]

1.5 Computational insights of liquids for gas separations

Molecular dynamics (MD) simulates atomic or molecular interactions over time by applying Newton's second law of motion: for objects with constant mass, the rate of change of an object's velocity is proportional to the force applied to that object. The force acting on an atom in the simulation can be found from the potential energy, which is a function of the positions of all atoms. Mathematically, for a system with *N* atoms, this can be written as:

$$F_i = m_i \frac{dv_i}{dt} = m_i a_i \qquad F_i = -\frac{\partial}{\partial r_i} U(r^N) \qquad \text{(Eq. 1.1)}$$

where F_i of is the force acting on atom i, m_i is the mass of atom i, v_i is the velocity of atom i, t is time, and U is the potential energy as a function of r^N, the complete set of coordinates of $3N$ atomic coordinates. In essence, once the potential energy function is defined, one only needs initial atomic positions and velocities to begin a molecular dynamics trajectory.

Modeling the bulk phase of a liquid tends to require a large number of atoms or molecules in order to get a realistic simulation. For this reason, quantum mechanical (QM) calculations, which describe electronic behavior, might be too computationally expensive depending on the information one wants to find for a given system. CMD methods are faster, as they employ force fields (FFs) which define bond lengths, angles, dihedrals, and more to describe interatomic interactions, and when done with a GPU, can be even faster to perform. CMD of course has its own limitations, a large one being the inability to form or break chemical bonds in a simulation. Neither method is inherently better than the other, they are simply different approaches for answering different questions.

Because this work looks at large-scale systems, modeling bulk liquids with thousands of atoms, we primarily employ CMD methods. The limitation mentioned before is not necessarily a major concern, however, as we study materials which physisorb—rather than chemisorb—small gas molecules, as mentioned in the previous sections. While QM methods are more precise in capturing the energetics of a chemical system, we can tune our CMD parameters to match them within reason, adjusting the FFs we define for a molecule's bond lengths, bond angles, etc. Moreover, comparing

simulations to experimental data allows us to judge how accurate a computational method may be for the system studied and similar situations. The CMD simulations provide us with structural and dynamics information about our systems, and describe interactions between atoms and molecules, which we use to better understand the mechanisms involved in gas separation media. Along with CMD, we utilize other computational methods, such as the statistical-mechanical Monte Carlo method to predict gas uptakes and umbrella sampling to calculate free energy changes, which is addressed in later chapters.

1.6 General Amber Force Field

The FF we primarily employ in this work is the general Amber force field (GAFF), developed by Wang and coworkers.[22] GAFF was designed to be used on organic molecules, describing molecules consisting of H, C, N, O, S, P, and halogens, which covers the systems we do in this work, with a few minor and simple exceptions. Much of GAFF is built off of previous Amber FFs, with additional empirical and ab initio information. The basic functional form of GAFF is written as:

$$E_{pair} = \sum_{bonds} k_r(r - r_{eq})^2 + \sum_{angles} k_\theta(\theta - \theta_{eq})^2 + \sum_{dihedrals} \frac{v_n}{2} \times [1 + cos(n\phi - \gamma)] + \sum_{i<j}\left[\frac{A_{ij}}{R_{ij}^{12}} - \frac{B_{ij}}{R_{ij}^{6}} + \frac{q_i q_j}{\varepsilon R_{ij}}\right] \quad \text{(Eq. 1.2)}$$

where r_{eq} and θ_{eq} are equilibrium structure parameters, k_r, k_θ, and v_n are force constants, n is multiplicity, γ is the phase angle for torsional angle parameters, and A, B, and q are nonbonded potential parameters.[22]

Reference bond lengths (r_{eq}) were derived from crystal structures and MP2/6-31G* optimizations of organic molecules. The bond length force constants (k_r) were determined by these reference bond lengths and force constants from the Amber protein force field. The developers acknowledge that this choice is risky, depending on previous parameterization, but test sets show a low percent error of 1.6% compared to experimental vibrational spectra.[22] Reference bond angles (θ_{eq}) and force constants (k_θ) were similarly derived from crystallographic data, ab initio calculations, and previous force fields, with an average percent error of 9.0% in the test cases.[22] Dihedral force constant (v_n) parameterization was performed by fitting to ab initio torsional angle scans of 200 model molecules.[22] A great benefit of GAFF is that it is a complete force field as it determines parameters for any atom combination algorithmically, rather than calling from a set list, allowing one to describe uncommon organic molecules.

1.7 References

1. Scholl, D. S.; Lively, R .P. Seven chemical separations to change the world. *Nature* **2016**, *532*, 435–437.

2. Aaron, D.; Tsouris, C. Separation of CO_2 from Flue Gas: A Review. *Sep. Sci. Technol.* **2005**, *40*, 321−348.

3. Lee, J.; Kim, J.; Hyeon, T. Recent progress in the synthesis of porous carbon materials. *Adv. Mater.* **2006**, *18*, 2073–2094.

4. Long, J. R.; Yaghi, O. M. The pervasive chemistry of metal-organic frameworks. *Chem. Soc. Rev.* **2009**, *38*, 1213–1214.

5. Eddaoudi, M.; Kim, J.; Rosi, N.; et al. Systematic design of pore size and functionality in isoreticular MOFs and their application in methane storage. *Science* **2002**, *295*, 469–472.

6. Diercks, C. S.; Yaghi, O. M. The atom, the molecule, and the covalent organic framework. *Science* **2017**, *355*, 1585.

7. Anthony, J.L.; Maginn, E.J.; Brennecke, J.F. Solution Thermodynamics of Imidazolium-Based Ionic Liquids and Water. *J. Phys. Chem. B* **2001**, *105*, 10942−10949.

8. Brennecke, J.F.; Gurkan, B.E. Ionic liquids for CO_2 capture and emission reduction. *J. Phys. Chem. Lett.* **2010,** *1,* 3459-3464.

9. Noble, R.D.; Gin, D.L. Perspective on ionic liquids and ionic liquid membranes. *J. Membr. Sci.* **2011,** *369,* 1-4.

10. Zeng, S.; Zhang, X.; Bai, L.; Zhang, X.; Wang, H.; Wang, J.; Bao, D.; Li, M.; Liu, X.; Zhang, S. Ionic-liquid-based CO_2 capture systems: Structure, interaction, and process. *Chem. Rev.* **2017,** *117,* 9625-9673.

11. Gurkan, B.; Goodrich, B.F.; Mindrup, E.M.; Ficke, L.E.; Massel, M.; Seo, S.; Senftle, T.P.; Wu, H.; Glaser, M.F.; Shah, J.K.; et al. Molecular Design of High Capacity, Low Viscosity, Chemically Tunable Ionic Liquids for CO_2 Capture. *J. Phys. Chem. Lett.* **2010**, *1*, 3494−3499.

12. Seo, S.; Quiroz-Guzman, M.; DeSilva, M. A.; et al. Chemically Tunable Ionic Liquids with Aprotic Heterocyclic Anion (AHA) for CO_2 Capture. *J. Phys. Chem. B* **2014***, 118,* 5740−5751.

13. O'Reilly, N.; Giri, N.; James, S. L. Porous liquids. *Chem. Eur. J.* **2007**, *13*, 3020–3025.

14. Hasell, T.; Cooper, A. I. Porous organic cages: soluble, modular and molecular pores. *Nat. Rev. Mater.* **2016**, *1*, 16053.

15. Giri, N.; Davidson, C. E.; Melaugh, G.; et al. Alkylated organic cages: from porous crystals to neat liquids. *Chem. Sci.* **2012**, *3*, 2153–2157.

16. Melaugh, G.; Giri, N.; Davidson, C. E.; et al. Designing and understanding permanent microporosity in liquids. *Phys. Chem. Chem. Phys.* **2014**, *16*, 9422–9431.

17. Giri, N.; Del Pópolo, M.; Melaugh, G.; et al. Liquids with permanent porosity. Nature **2015**, *527*, 216–220.

18. Zhang, J.; Chai, S.-H.; Qiao, S.-H.; et al. Porous liquids: a promising class of media for gas separation. *Angew. Chem. Int. Ed.* **2015**, *54*, 932–936.

19. Li, P.; Schott, J. A.; Zhang, J.; et al. Electrostatic-assisted liquefaction of porous carbons. *Angew. Chem. Int. Ed.* **2017**, *56*, 14958–14962.

20. Caira, M. R.; Bourne, S. A.; Mhlongo, W. T.; et al. New crystalline forms of permethylated β-cyclodextrin. *Chem. Comm.* **2004**, 2216.

21. Alsbaiee, A.; Smith, B. J.; Xiao, L.; et al. Rapid removal of organic micropollutants from water by a porous β-cyclodextrin polymer. *Nature* **2015**, *529*, 190-194.

22. Wang, J.; Wolf, R.M.; Caldwell, J.W.; Kollman, P.A.; Case, D.A. Development and Testing of a General Amber Force Field. *J. Comput. Chem.*, **2004**, *25*, 1157.

CHAPTER TWO

Molecular Dynamics Simulations of a Dicationic Ionic Liquid for CO_2 Capture

2.1 Abstract

A dicationic ionic liquid ([DBU-PEG][Tf_2N]$_2$) was studied using classical molecular dynamics simulations to examine its structural and gas separation properties. The dication was designed in an attempt to improve CO_2 solubility by means of tuning the cation-anion interactions of the ionic liquid (IL). The computational model was compared to experimentally obtained density, viscosity, and powder x-ray diffraction spectra. The structure of the IL was further investigated with radial distribution functions and free volume analysis through cavity distributions. It was found that the shape and charge distribution of the dication enhances CO_2 interaction: the CO_2 molecule is hugged by the dication along the PEG linker and close to one of the cationic ends. The geminal design of the dication allows for strong interaction with CO_2, showing promise as a means of carbon capture.

2.2 Introduction

As greenhouse gas emissions continue to rise, the need for effective gas separation and carbon capture materials increases as well. Separation of CO_2 from air or other post-combustion gases is desirable not just in an environmental sense, but also for applications in the synthesis of other organic compounds.[1-4] Ionic liquids (ILs), noted for their low vapor pressures and melting points at or below room temperature, are of

particular interest as a medium for gas separations as ILs may easily be tuned in terms of solubility and selectivity of CO_2, by means of altering the cationic and anionic components.[5-6] Imidazolium-based ILs are the popular choice for CO_2 separation, but the extensive list of IL species leaves many to still be explored.[7]

In general, the anion is the primary contributor tuning the solubility of CO_2, while the cation tends to have a less significant effect.[8-10] However, due to its large quadrupole moment, the partial negative charges on the O of CO_2 may interact with the IL's cationic centers. This interaction is enhanced when the cation-anion charge interactions are weaker, as previous studies of gas behaviors in ILs show that a weaker charge interaction allows for higher solubility of CO_2.[8]

Given the importance of cation-anion interactions in impacting gas solubility and diffusivity in ILs, an obvious knob to tune is the charge valence on the ions. This can be done by distributing charge density to a wider area of the ion. Symmetric, or geminal, dications in ILs, which feature two cationic centers, usually spaced by an alkyl chain, have been studied for gas separations.[11-13] Having a larger dication raises the viscosity of the liquid, significantly lowering permeability of gases, however, this effect may be lessened by using an oligoether chain rather than an alkyl group.[14-15]

The dication applied in this work is glycol-bonded 1,8-diazabicyclo-[5.4.0]undec-7-ene ($[DBU\text{-}PEG]^{2+}$). Coupled with the bis(trifluoromethylsulfonyl)imide (Tf_2N^-) anion, this IL (Figure 2.1) has been studied experimentally as a solvent for ZIF-8, acting as a porous liquid used for gas separation.[16] The advantage of this IL is its higher CO_2 solubility at ambient conditions (0.22 $mol \cdot L^{-1}$ at 1 atm), in comparison with the most

popular IL systems such as [EMIM][Tf_2N] (0.10 mol·L^{-1} at 1 atm) and the ionic liquids with the [$B(CN)_4$] anion known for their high CO_2 solubility (for example, 0.13 mol·L^{-1} at 1 atm in [EMIM][$B(CN)_4$]).[2,8-9,16]

Although the Tf_2N^- anion is common in ILs, the design of the [DBU-PEG]$^{2+}$ dication is more unique. The cationic centers come from DBU groups, a bicyclic amidine, which is bulkier than planar imidazolium-based cations common in ILs. This added bulk allows for a higher free volume, effectively easing the addition of solutes like CO_2.[17-19] The DBU groups are tethered by a PEG linker, which, when compared to alkyl-chain analogs, has been shown to increase selectivity for CO_2 over N_2 or CH_4, making for a distinct cation worth investigating.[20] Hence, the goal of this work is to understand the structure and dynamics of the [DBU-PEG][Tf_2N]$_2$ IL and its interaction with CO_2 from classical molecular dynamics simulations.

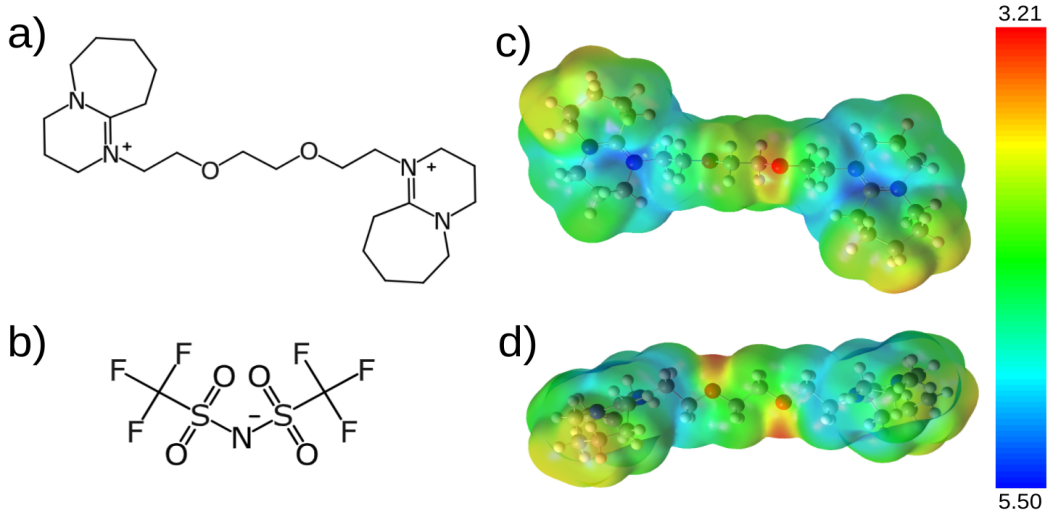

Figure 2.1 Chemical structures of (a) the [DBU-PEG]$^{2+}$ dication and (b) the bis(trifluoromethylsulfonyl)imide (Tf_2N^-) anion. (c) Top and (d) side views of electrostatic potential (in eV) of [DBU-PEG]$^{2+}$ mapped to an electron-density isosurface of 0.0004 e^-/a_o^3.

2.3 Computational Details

Classical molecular dynamics simulations were performed using the Amber 16 program.[21] A periodic box housed 38 $[DBU\text{-}PEG]^{2+}$ dications, 76 Tf_2N^- anions, and a varying number of CO_2 molecules ranging from 0 to 14 (mole fraction equal to 0% to 10.9%, respectively). These molecular fractions match the experimentally measured solubility: at 10 atm, the measured value is about 0.35 mmol CO_2 per gram of the IL,[16] which corresponds to 0.34 mol CO_2 per mol of the IL; we simulated up to 14 CO_2 molecules in 38 formula units of the IL or 0.38 mol CO_2 per mol of the IL. The initial packing of the box was done with Packmol.[22] Five simulations with random starting configurations were performed at each concentration of CO_2 to ensure that results were consistent. All force field parameters were built using the general Amber force field (GAFF).[23] Partial atomic charges were generated from the restricted electrostatic potential (RESP) method based on molecular geometries optimized at the B3LYP/6-311G(d) level using Gaussian 09.[24]

The systems were minimized before heating to 300 K over 1 ns. Constant number, pressure, and temperature (NPT) simulations ran for 30 ns at 300 K, though the first 15 ns are treated as equilibration steps and were not used for analysis. Similarly, constant number, volume, and temperature (NVT) simulations of 30 ns followed, using only the final 15 ns for analysis. NPT simulations are necessary for equilibrating to a suitable simulation box size, and therefore density, as the boundaries are allowed to vary. Density of the ionic liquid was determined with the averaged simulation box volume from the final 15 ns of NPT simulations.

Cavity distributions were calculated by generating 1000 random points in each frame of the simulation, and finding the largest sphere that would fit at that point without touching an atom (defined by its van der Waals radius used in the force field) in the frame. The diameters of these spheres were plotted as a probability distribution. Simulated powder x-ray diffraction (XRD) spectrum and viscosity prediction were obtained with Materials Studio by Biovia, using frames taken from the NVT simulation.[25] Peaks of the simulated XRD spectrum, with a copper x-ray wavelength of 1.54 Å, were broadened with gaussian distributions to present more like an amorphous material rather than a crystal. Shear viscosity calculations were performed with the NVT ensemble, at 298 K, with a shear rate of 0.1 ps^{-1}, and using the partial charges produced via the RESP method.

Synthesis of the IL was done following the same methods performed by Shan et al.[16] Experimental viscosity measurements were obtained using a Brookfield DVII+ Pro cone plate viscometer. Powder X-ray diffraction (XRD) patterns were collected on a PANalytical Empyrean diffractometer with Ni-filtered Cu Kα (λ = 1.54 Å) radiation operating at 45 kV and 40 mA.

2.4 Results and Discussion

2.4.1 Validation through density and viscosity. To assess the validity of our methods and model used, we compare predicted values to experimental observables. Density and viscosity are compared in Table 1, with good agreement between experiment and

simulation. These comparisons to experiment are encouraging in gauging the reliability of our modeling methods.

Table 2.1 Density and viscosity of [DBU-PEG][Tf_2N]$_2$ from simulation and experiment.

	Simulation	**Experiment**
Density (g/mL)	1.455	1.448
Viscosity (cP)	1608	1888

2.4.2 Structure. A simulated XRD spectrum is shown in Figure 2.2 with peaks marked symbolically. In the spectrum, there is a major peak, α, at 18.5°, and a short and broad peak, β, at 37.0°. Applying Bragg's law, with a copper x-ray wavelength of 1.54 Å, we find that the peaks α and β correspond to spacings of 4.79 Å and 2.43 Å, respectively. However, the β peak is considered to be an overtone of the α peak, as Bragg's law includes an integer n, the order of reflection. In this case, the α peak corresponds to n=1, whereas the β peak is a result of n=2. To reveal the atomistic origins of the 4.79 Å peak, in the following we analyze radial distribution functions (RDFs) that give insight into the structure of the liquid and the ion-ion interactions.

In Figure 2.3 we include the RDF of the cation-center around a central carbon of the PEG chain, with a large peak at 4.88 Å which corresponds to the broad α peak and shoulder seen in the XRD spectra. Figure 2.4 shows the RDFs of the anionic center of Tf_2N^- around one cationic center of $[DBU\text{-}PEG]^{2+}$ and a cationic center of one $[DBU\text{-}PEG]^{2+}$ around a cationic center of a neighboring $[DBU\text{-}PEG]^{2+}$. The

anion-to-one-cation-center distance shows two close peaks at 5.6 and 6.2 Å. The inter-ion cation-center-to-cation-center RDF shows a small peak at 4.9 Å, a much higher probability after 6.0 Å, and then a broad peak at about 9.4 Å.

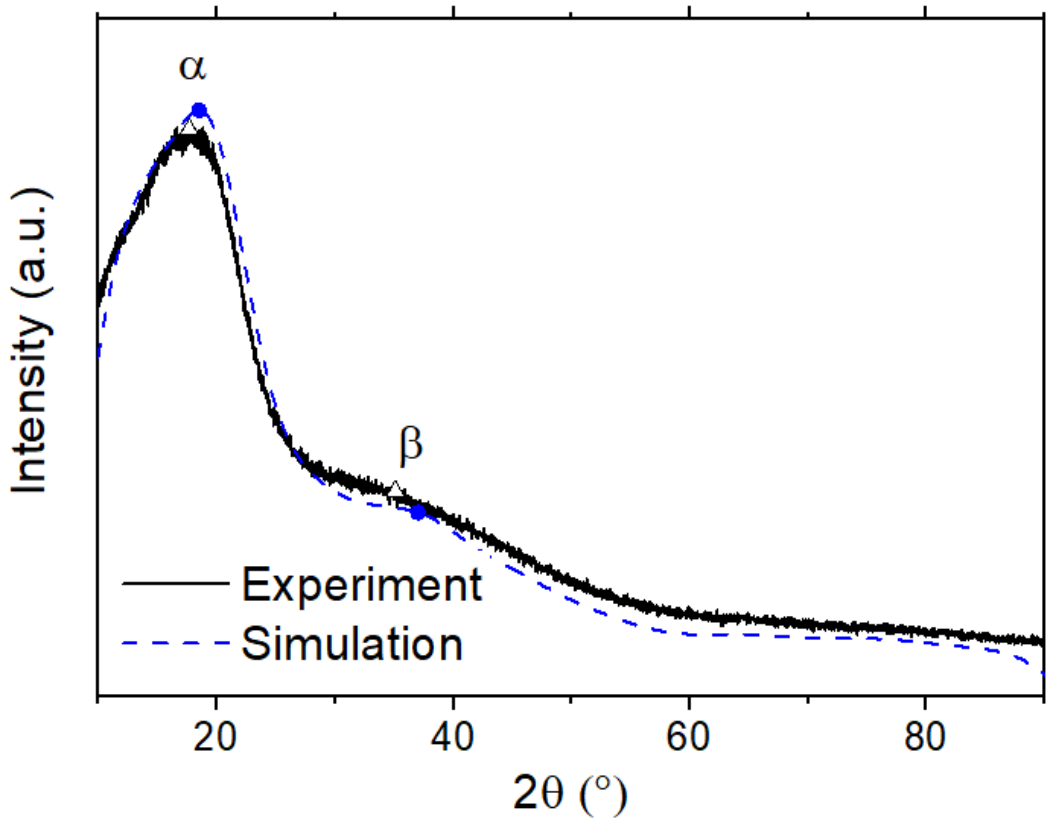

Figure 2.2 Simulated (blue dashed) and experimental (black solid) powder x-ray diffraction patterns of the [DBU-PEG][Tf_2N]$_2$ IL.

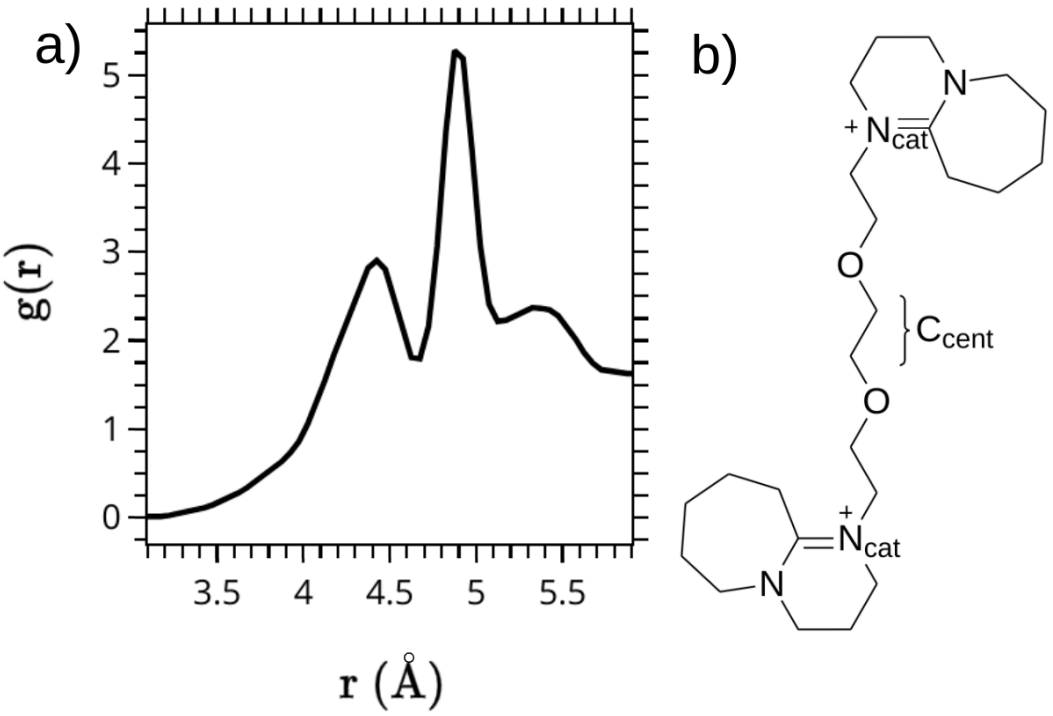

Figure 2.3 (a) Radial distribution function of cationic centers, N_{cat}, around central carbons, C_{cent}, of PEG linker. (b) Molecular structure of $[DBU\text{-}PEG]^{2+}$ with N_{cat} and C_{cent} labeled.

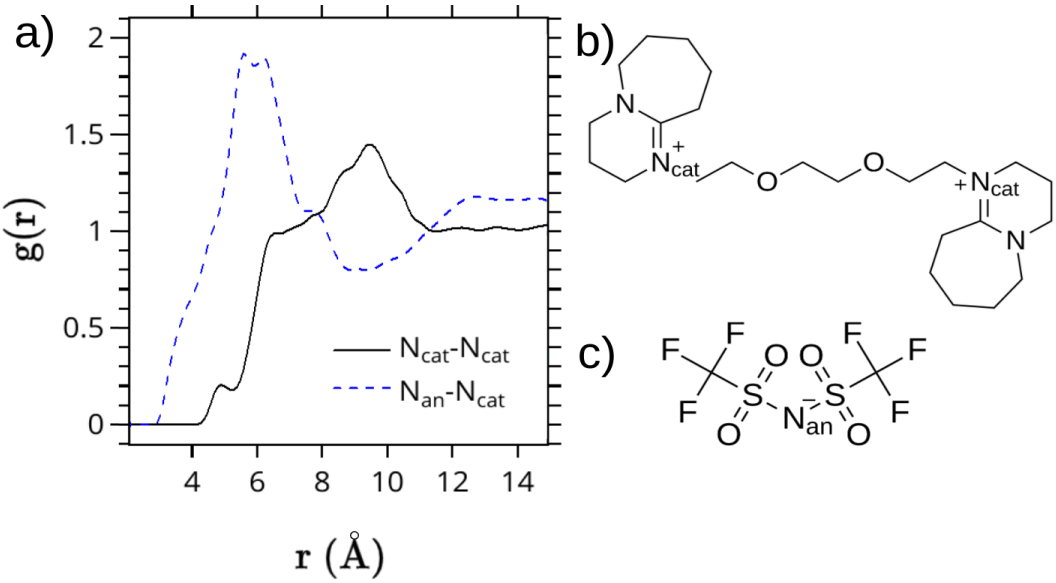

Figure 2.4 (a) Radial distribution functions of the anionic center, N_{an}, of Tf_2N^- around one cationic center, N_{cat}, of $[DBU\text{-}PEG]^{2+}$ (blue dashed) and a cationic center of one $[DBU\text{-}PEG]^{2+}$ around a cationic center of a neighboring $[DBU\text{-}PEG]^{2+}$ (black solid) in the $[DBU\text{-}PEG][Tf_2N]_2$ IL. (b) $[DBU\text{-}PEG]^{2+}$ with N_{cat} labeled; (c) TfN_2^- with N_{an} labeled.

Figure 2.5 shows the intra-ion cation-center-to-cation-center RDF, which can also be thought of as the distance between the two cationic centers on a single dication. One can see that there are two distinct peaks at 7.30 and 9.25 Å. We found that they correspond to two major conformations of $[DBU\text{-}PEG]^{2+}$ in the IL. As pictured in the figure, the dication can take either a compressed or outstretched conformation, corresponding to the peaks at 7.30 and 9.25 Å, respectively.

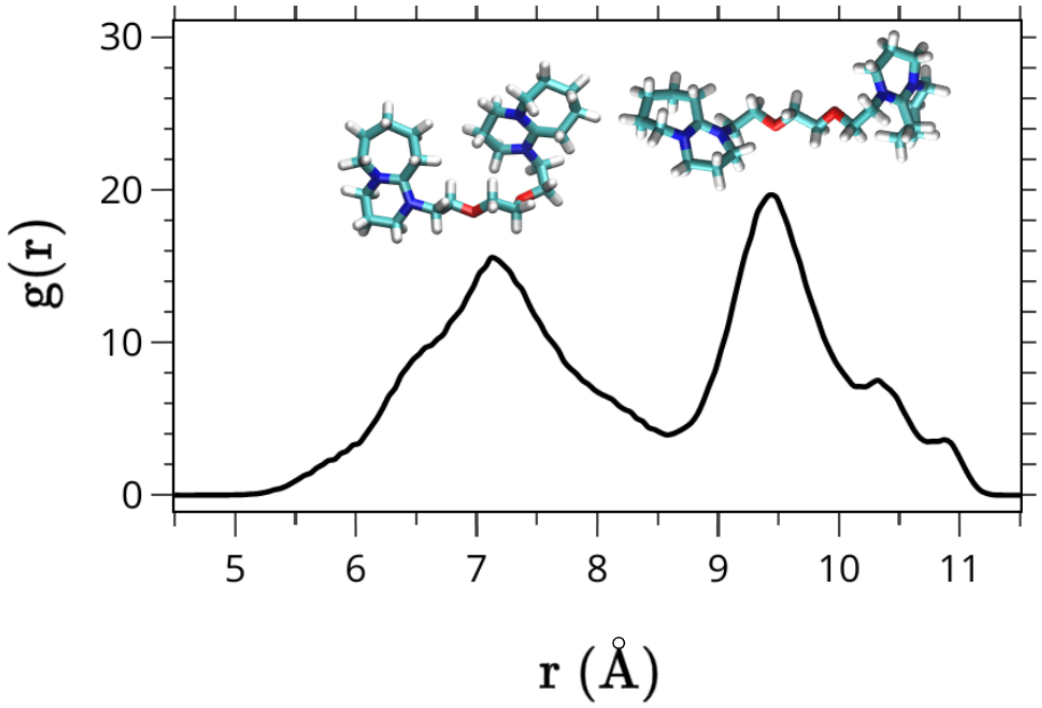

Figure 2.5 Radial distribution function of one cationic center, N_{cat}, to the other on the same $[DBU\text{-}PEG]^{2+}$ with corresponding conformations shown above each peak.

2.4.3 Cavity distribution. An important factor in gauging the ability of a liquid to uptake gases is the free volume. Cavity distributions are a representation of the free volume, as it measures the average size of cavities within the liquid. Figure 2.6 shows the cavity distribution of the $[DBU\text{-}PEG][Tf_2N]_2$ IL. The cavity sizes follow a close-to-normal

probability distribution, with an average diameter of 2.70 Å. About 22.7% of the cavities existing in the IL are large enough to accommodate CO_2 whose kinetic diameter is indicated by a dashed line in Figure 2.6.[26] Here we note that this is just a rough estimate, as the cavity distribution would change with CO_2 concentration in the ionic liquid; the size of the CO_2 molecule, however, is expected to stay close to its kinetic diameter which matches the cross-sectional diameter of CO_2 molecule's electron cloud.[26] The solvation environment of the ionic liquid might slightly distort or polarize CO_2's electron cloud, but on average we do not expect the size of the CO_2 molecule would vary much, given the physisorption nature of CO_2 in this ionic liquid. Next, we examine how CO_2 molecules occupy these larger cavities.

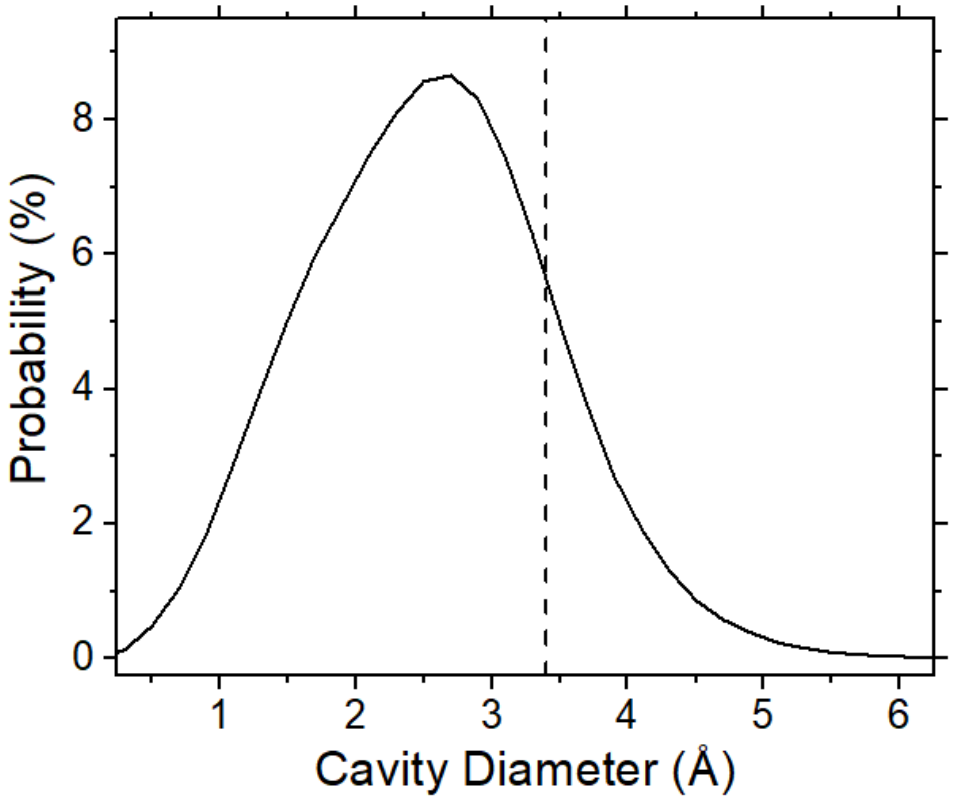

Figure 2.6 Cavity distribution in the [DBU-PEG][Tf_2N]$_2$ IL. Dashed line marks kinetic diameter of CO_2.

2.4.4 Structure of CO_2 in the [DBU-PEG][Tf_2N]$_2$ IL. When CO_2 is introduced, we see an interesting interaction between the $[DBU\text{-}PEG]^{2+}$ and CO_2. Figure 2.7 shows the spatial distribution function (SDF) of CO_2 around a dication molecule: for the extended conformation (Figure 2.7a), CO_2 tends to dwell along the central PEG linker of the extended dication, and generally avoids the outer edges; for the compressed conformation (Figure 2.7b), CO_2 tends to be on the side and facing one cationic ring, in addition to

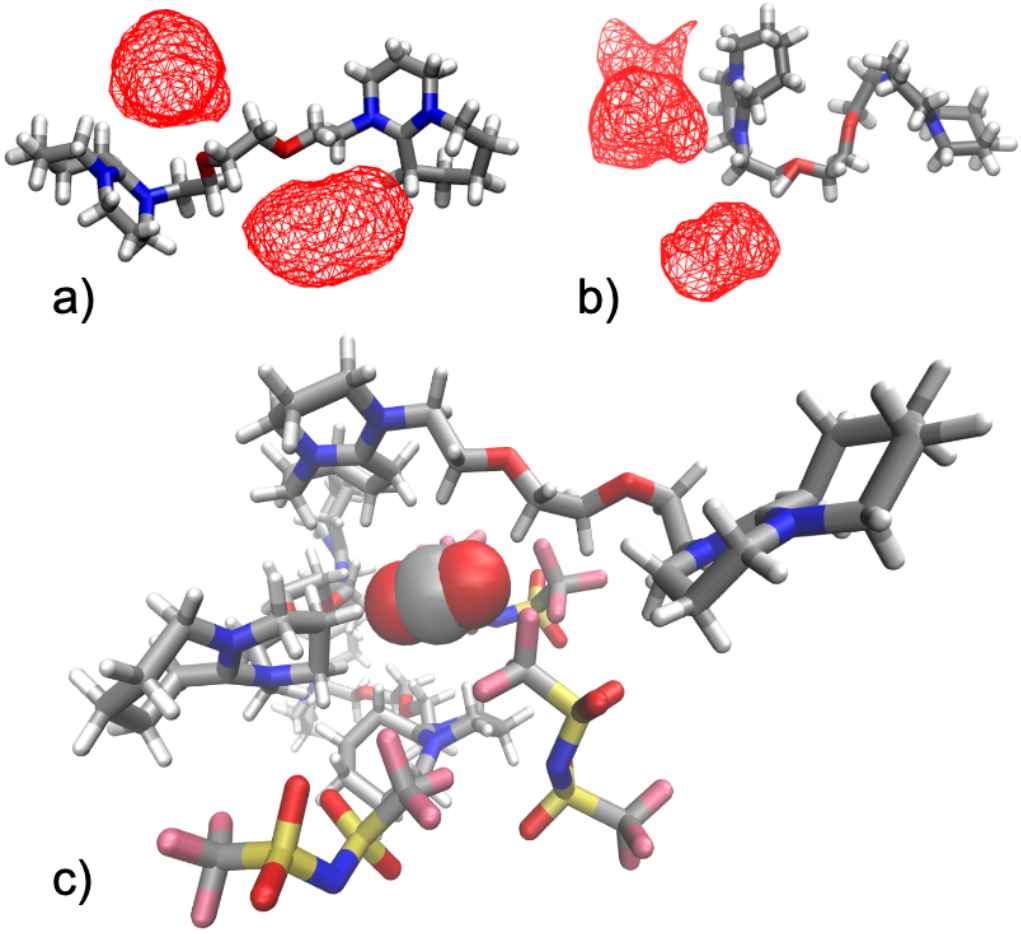

Figure 2.7 Spatial distribution function of CO_2 (red wireframe) around the extended conformation (a) and compressed conformation (b) of $[DBU\text{-}PEG]^{2+}$ and a representative snapshot of the solvation environment of CO_2 in [DBU-PEG][Tf_2N]$_2$ IL with CO_2 mole fraction of 1.7%.

some distribution next to the PEG linker. As indicated in Figure 2.1, the ESP surface of the dication has both the more positive (blue) DBU groups and the more negative (red) PEG linker. Hence, the positive centers can interact with the negatively charged O atoms of CO_2, while the negative centers from the PEG are attracted to the positive C atom of CO_2. Figure 2.7c shows a representative snapshot of CO_2's solvation environment: one can see that CO_2 is interacting with both the dication's DBU groups and the PEG linker as well as with the anions. Figure 2.8a shows the RDF of the O atoms on CO_2 to the nearest hydrogen atoms on a DBU group and one can clearly see their close contact between 2.3 and 2.4 Å, as manifested in a typical snapshot of such interaction in Figure 2.8b.

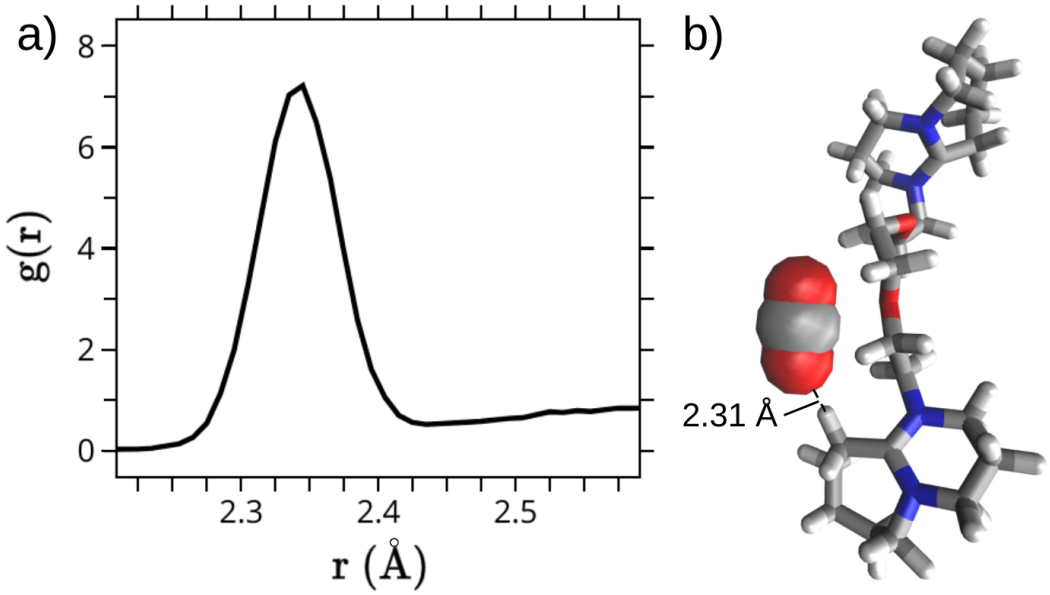

Figure 2.8 Interaction of DBU hydrogens with CO_2 oxygen in the [DBU-PEG][Tf_2N]$_2$ IL with CO_2 mole fraction of 1.7%: (a) radial distribution function of DBU hydrogens around CO_2 oxygen; (b) a representative snapshot showing close interaction of a DBU hydrogen (white) and a CO_2 oxygen (red sphere).

2.4.5 Energetics of CO_2 in the [DBU-PEG][Tf_2N]$_2$ IL. The experimentally measured solubility of CO_2 in [DBU-PEG][Tf_2N]$_2$ is 0.15 mmol·g^{-1} or 0.22 mol·L^{-1} at 1 atm,[16] among the highest for ionic liquids that physisorb CO_2, including popular IL systems based on imidazolium cations and Tf_2N^- and other anions such as $B(CN)_4^-$.[2,5-6,8-9] Physisorption refers to the fact that there is no bonded interaction between CO_2 and the moieties of the IL, as our simulations have shown and further reflected in the interaction energy. We have computed the interaction energy of CO_2 with the dication at the MP2/6-31G level of theory and found a favorable interaction energy of -36 kJ/mol which is consistent with the high solubility of CO_2 in in [DBU-PEG][Tf_2N]$_2$. We think that the dication approach can be further expanded by exploring other dications, for example, by varying the PEG linker length. In addition, one envisions that composite materials such as porous liquids built upon such dication ILs could offer new opportunities in capturing CO_2 either as membranes or sorbents.

2.5 Conclusions

We have investigated a dicationic ionic liquid, [DBU-PEG][Tf_2N]$_2$, for capturing CO_2 through classical molecular dynamics. Simulated XRD and RDFs were used to characterize the structure of the liquid. Upon analysis of the neat liquid, the dication is shown to take on two major conformations in the simulation, one which is compressed along the linker, and one which is outstretched. The dication's PEG linker appears to separate the cationic centers from the anions, weakening the ionic interactions of the IL. The free volume of the IL is assessed through cavity distributions, showing that in the

liquid there exists a good deal of cavities large enough to accommodate CO_2. Simulations of CO_2 in the IL revealed favorable interaction of CO_2 with the dication, enhanced by the shape and charge distribution of the dication. The CO_2 tends to be hugged by the dication along the PEG linker, with one CO_2 oxygen coordinated to one of two DBU groups. Combining the features of a bicyclic amidine and the geminal design, this dication inspires further tuning of ILs for gas separation. Because gas separation in ILs has been shown to be heavily influenced by the anion, future studies featuring a similar design approach for a bulky dianion may be worth investigating as well.

2.6 References

1. Schrag, D.P. Preparing to Capture Carbon. *Science,* **2007**, *315*, 812.

2. Bara, J.E.; Carlisle, T.K.; Gabriel, C.J.; Camper, D.; Finotello, A.; Gin, D.L.; Noble, R.D. Guide to CO_2 Separations in Imidazolium-Based Room-Temperature Ionic Liquids. *Ind. Eng. Chem. Res.* **2009,** *48,* 2739.

3. Sakakura, T.; Choi, J.C.; Yasuda, H. Transformation of Carbon Dioxide. *Chem. Rev.* **2007,** *107*, 2365.

4. Liu, Q.; Wu, L.; Jackstell, R.; Beller, M. Using Carbon Dioxide as a Building Block in Organic Synthesis. *Nat. Commun.* **2015,** 6, 5933.

5. Lei, Z.; Dai, C.; Chen, B. Gas Solubility in Ionic Liquids. *Chem. Rev.* **2014,** *114,* 1289.

6. Hu, Y.F.; Liu, Z.C.; Xu, C.M.; Zhang, X.M. The Molecular Characteristics Dominating the Solubility of Gases in Ionic Liquids. *Chem. Soc. Rev.* **2011,** *40*, 3802.

7. Liu, H.; Dai, S.; Jiang, D.E. Solubility of Gases in a Common Ionic Liquid from Molecular Dynamics Based Free Energy Calculations. *J. Phys. Chem. B,* **2014,** *118,* 2719.

8. Babarao, R.; Dai, S.; Jiang, D.E. Understanding the High Solubility of CO_2 in an Ionic Liquid with the Tetracyanoborate Anion. *J. Phys. Chem B,* **2011,** *115,* 9789.

9. Mahurin, S.M.; Lee, J.S.; Baker, G.A.; Luo, H.; Dai, S. Performance of Nitrile-containing Anions in Task-Specific Ionic Liquids for Improved CO_2/N_2 Separation. *J. Membr. Sci.* **2010,** *353*, 177.

10. Aki, S.N.V.K.; Mellein, B.R.; Saurer, E.M.; Brennecke, J.F. High-pressure Phase Behavior of Carbon Dioxide with Imidazolium Based Ionic Liquids. *J. Phys. Chem. B,* **2004,** *108*, 20355.

11. Bara, J.E.; Hatakeyama, E.S.; Gabriel, C.J.; Zeng, X.; Lessmann, S.; Gin, D.L.; Noble, R.D. Synthesis and Light Gas Separations in Cross-Linked Gemini Room Temperature Ionic Liquid Polymer Membranes. *J. Membr. Sci.* **2008,** *316,* 186.

12. Shahkaramipour, N.; Adibi, M.; Seifkordi, A.A.; Fazli, Y. Separation of CO_2/CH_4 Through Alumina-Supported Geminal Ionic Liquid Membranes. *J. Membr. Sci.* **2014,** *455*, 229.

13. Li, S.; Zhao, W.; Feng, G.; Cummings, P.T. A Computational Study of Dicationic Ionic Liquids/CO_2 Interfaces. *Langmuir,* **2015**, *31*, 2447.

14. Siqueira, L.J.A.; Ribeiro, M.C.C. Alkoxyl Chain Effect on the Viscosity of a Quaternary Ammonium Ionic Liquid: Molecular Dynamics Simulations. *J. Phys. Chem. B,* **2009,** *113*, 1074.

15. Chen, Z.J.; Xue, T.; Lee, J.M. What Causes the Low Viscosity of Ether-Functionalized Ionic Liquids? Its Dependence on the Increase of Free Volume. *RSC Adv.* **2012,** *2,* 10564.

16. Shan, W.; Fulvio, P.F.; Kong, L.; Schott, J.A.; Do-Thanh, C.L.; Tian, T.; Hu, X.; Mahurin, S.M; Xing, H.; Dai, S. New Class of Type III Porous Liquids: A Promising Platform for Rational Adjustment of Gas Sorption Behavior. *ACS Appl. Mater. Interfaces* **2018,** *10*, 32.

17. Shannon, M.S.; Tedstone, J.M.; Danielsen, S.P.O.; Hindman, M.S.; Irvin, A.C.; Bara, J.E. Free Volume as the Basis of Gas Solubility and Selectivity in Imidazolium-Based Ionic Liquids. *Ind. Eng. Chem. Res.* **2012,** *51*, 5565.

18. Schott, J.A.; Do-Thanh C.L.; Mahurin, S.M.; Tian, Z.; Onishi, N.C.; Jiang, D.E.; Dai, S. Supported Bicyclic Amidine Ionic Liquids as a Potential CO_2/N_2 Separation Medium. *J. Membr. Sci.* **2018,** *565,* 203.

19. Klähn, M.; Seduraman, A. What Determines CO_2 Solubility in Ionic Liquids? A Molecular Simulation Study. *J. Phys. Chem. B,* **2015**, *119*, 10066.

20. Bara, J.E.; Gabriel, C.J.; Lessmann, S.; Carlisle, T.K.; Finotello, A.; Gin, D.L.; Noble, R.D. Enhanced CO_2 Separation Selectivity in Oligo(ethylene glycol) Functionalized Room-Temperature Ionic Liquids. *Ind. Eng. Chem. Res.* **2007,** *46*, 5380.

21. Case, D.A.; Betz, R.M.; Cerutti, D.S.; Cheatham, T.E., III; Darden, T.A.; Duke, R.E.; Giese, T.J.; Gohlke, H.; Goetz, A.W.; Homeyer, N.; et al. **2016**, AMBER 2016, University of California, San Francisco.

22. Martínez, L.; Andrade, R.; Birgin, E.G.; Martínez, J.M. Packmol: A Package for Building Initial Configurations for Molecular Dynamics Simulations. *J. Comput. Chem.* **2009**, *30*, 2157.

23. Wang, J.; Wolf, R.M.; Caldwell, J.W.; Kollman, P.A.; Case, D.A. Development and Testing of a General Amber Force Field. *J. Comput. Chem.*, **2004**, *25*, 1157.

24. Frisch, M.J.; Trucks, G.W.; Schlegel, H.B.; Scuseria, G.E.; Robb, M.A.; Cheeseman, J.R.; Scalmani, G.; Barone, V.; Petersson, G.A.; Nakatsuji, H.; et al. **2016**, Guassian 09, Gaussian, Inc., Wallingford, CT.

25. Dassault Systèmes BIOVIA, Materials Studio 5.0, San Diego: Dassault Systèmes, **2017**.

26. Mehio, N.; Dai, S.; Jiang, D.E. Quantum Mechanical Basis for Kinetic Diameters of Small Gaseous Molecules. *J. Phys. Chem. A*, **2014,** *118*, 1150.

2.7 Appendix

Because $[DBU\text{-}PEG]^{2+}$ has not been well-studied computationally, validation of the force field against quantum methods was necessary. This was done through geometric and energetic comparisons between the Amber code and B3LYP/6-311G(d). The cation was minimized in the gas state using both methods, and bond lengths, angles, and dihedral were compared, with relatively good agreement throughout. Bond lengths were within 0.02 Å, angles within 2.5°, and dihedrals within 8°, with the exception of those concerning the bridgehead carbon, placed between two nitrogens in the DBU groups. Even so, the differences in geometry for the carbons in question were still small, with bond lengths off by 0.08 Å, angles at 4°, and dihedrals around 12° off. The energy profile was assessed by a relaxed scan of the central PEG dihedral at the B3LYP/6-311G(d) level. In Amber, using the GAFF, single-point energies were calculated from the geometries found in the DFT scan. A comparison of the two methods is shown in Figure S2.1, and while the potential energy of the cis-conformation is underestimated by the GAFF by about 2.4 kcal/mol, the overall energy profiles agree well.

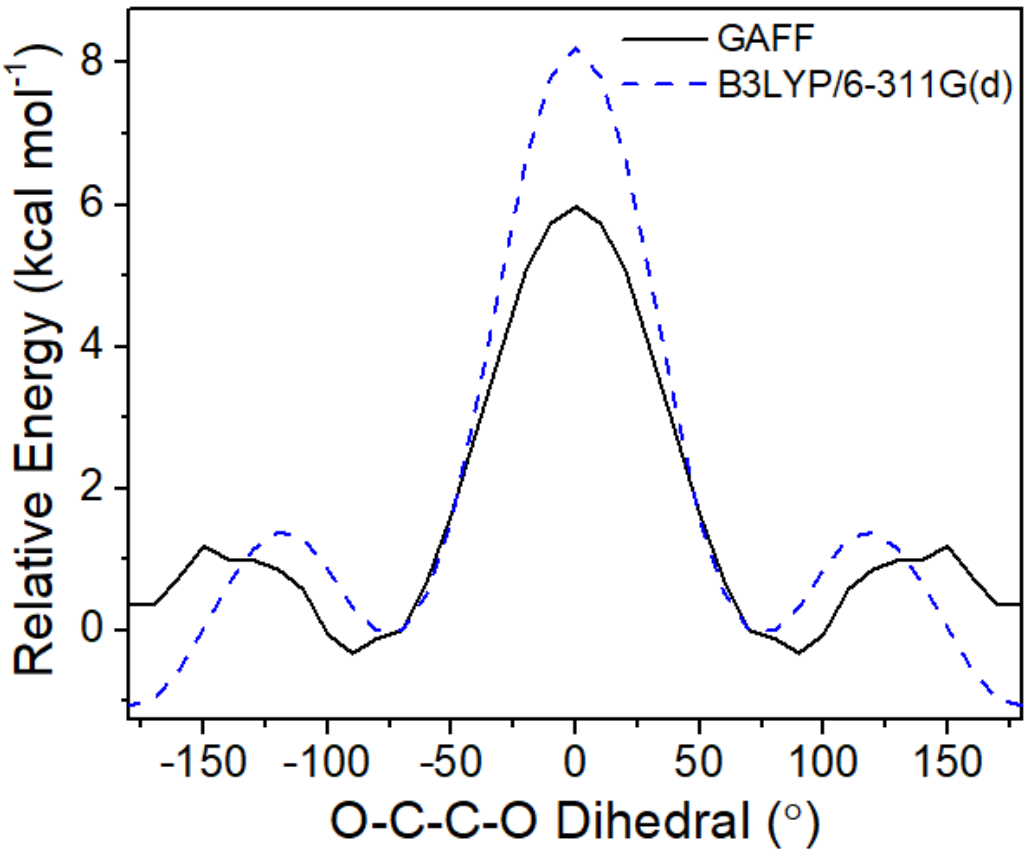

Figure S2.1 Potential energy surface of $[DBU\text{-}PEG]^{2+}$ twisted about the central PEG dihedral from GAFF (black solid) and DFT (blue dashed).

CHAPTER THREE

Computational Study of an Ionic Cage-based Porous Liquid for Gas Separation

3.1 Abstract

Classical molecular dynamics (MD) and other computational methods were used to study a new porous liquid (PL), composed of anionic covalent cages (ACC), lithium counterions, and 12-crown-4 ether. Powdered ACC is known to have a pore diameter of about 4.25 Å, so this PL was proposed as a material for gas separations. The interaction of small gas molecules, such as CO_2, CH_4, and N_2, with the ACC PL was studied, as well as the gases' solubility, diffusivity, and energetics. Although similar cage-based PLs have been studied computationally, a unique feature of the ACC PL is the single anionic carboxylate group creating an asymmetric structure. Spatial analysis of gases in the ACC PL showed asymmetric behavior as a result, with CO_2 and N_2 generally moving away from the carboxylate, and CH_4 preferring the areas closer to the carboxylate. Results also indicated that CO_2 capture was more favored than other gases tested, as CO_2 experienced longer times of stay within the pore of ACC molecules, as well as higher solubility and lower diffusivity.

3.2 Introduction

Gas separation and carbon capture methods continue to be an influential path in combating greenhouse gas emissions.[1,2] Carbon dioxide (CO_2) is the most prevalent greenhouse gas, emitted primarily through industrial processes and electricity production,

and effective capture of CO_2 through sorption poses a way to mitigate the release of greenhouse gases into the atmosphere. Sorption can be separated into two classes: chemisorption, in which a chemical bond is formed between the sorbate and sorbent, or physisorption, in which intermolecular forces are what hold the sorbate to the sorbent. Chemisorption typically has a large activation energy, so for sorbents to be used again and again, physisorption methods are preferred, as they require less energy input to regenerate.[3,4]

Common materials for gas separations and carbon capture include porous media, such as porous carbon, metal-organic-frameworks (MOFs), or zeolites.[5-8] One limitation of these traditional porous materials is that they are all solid at room temperature. For industrial procedures in which a continuous flow process would be preferred, solid porous materials are lacking. A new class of porous media was introduced by O'Reilly and coworkers in 2007, bringing about the concept of porous liquids (PLs).[9] A porous liquid is a liquid with permanent extrinsic porosity, meaning the cavities within the liquid are non-transient and generally uniform in size. PLs can be separated into three types: 1) neat liquids, 2) porous hosts dissolved in bulky solvents, and 3) frameworks dispersed in bulky solvents. In this work we propose a novel Type 1 PL, drawn in Figure 3.1, where an anionic covalent cage (ACC) is paired with an alkaline crown ether complex. This results in a liquid, while maintaining the porosity of the ACC. The inner pore of the ACC is approximately 4.25 Å in diameter, making this PL a suitable candidate for small gas molecule capture.[10]

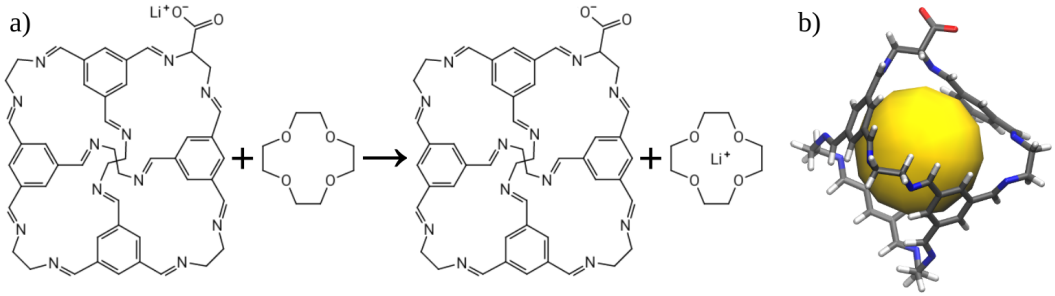

Figure 3.1 Design of ACC PL. a) Synthesis of ACC PL from powdered ACC and 12-crown-4 ether. b) Geometric structure of ACC with pore highlighted as a yellow sphere.

3.3 Computational Details

Chemical structures of all molecules were optimized in Gaussian 09 with the B3LYP functional and 6-311G(d) basis set, and partial charges were assigned from restricted electrostatic potential (RESP) charge fitting.[11] Force field parameters were assigned using the General Amber Force Field (GAFF) which is generally appropriate for organic molecules.[12] Although similar cage compounds in PLs have been computationally studied previously, the carboxylate group on the ACC is unique among other cage-based PLs. As a validation, a comparison of free energy profiles produced by the force field and quantum mechanical methods was performed, showing good agreement. Optimized geometries, force field parameters and other input files are included in the supplemental information.

Each simulation box began with 64 ACC, 64 Li^+, and 64 12-crown-4 ether molecules randomly packed into a 60 Å cube with Packmol.[13] For simulations with gases absorbed into the system, 16 CO_2, CH_4, or N_2 molecules were additionally randomly packed into the simulation box. The number of gas molecules was chosen so as not to exceed the predicted solubility at 1 bar. We ensured that in the initial coordinates the

ACC cavities were empty and that the box was not over-packed. Upon equilibration the 60 Å cube shrunk down to an approximately 48 Å box.

Classical molecular dynamics simulations of the PL with and without various gases absorbed were done using the Amber 16 code.[14] The periodic simulation boxes were minimized and heated to 300 K gradually over 1 ns. The simulations were given a 50 ns equilibration and production run with constant number, pressure, and temperature (NPT), allowing the simulation box to reach a reasonable size. Following this was a 50 ns production calculation with constant number, volume, and temperature (NVT). For both NPT and NVT production simulations, the first 25 ns were treated as equilibration steps and analysis was performed on only the final 25 ns.

Grand canonical Monte Carlo (GCMC) calculations were done to predict the adsorption isotherms of gases in ACC PL using Materials Studio software by Biovia.[15] Isotherms scanned pressures from 0.1 to 10 bar, and were done at both 298 K and 308 K. Langmuir fits were done on the isotherms to provide the equilibrium constant, K_{eq}, for each gas at both temperatures. From the predicted solubilities and the Clausius-Clapeyron equation, we were then able to calculate the heats of absorption (q_{st}) as a function of gas absorbed.

Analysis of MD trajectories was performed with a variety of tools, primarily within the AmberTools package.[14] Other analysis includes investigation of pore size, which was done by calculating the distance between the geometric center of an ACC molecule and the closest atom, taking into account the van der Waals radius of the closest atom. Free energy calculations of gas absorption into ACC were done with an umbrella

sampling method, and the potential of mean force (PMF) diagrams were stitched together with the Weighted Histogram Analysis Method (WHAM).[16] Applying the Einstein relation, $D = \frac{1}{6}\frac{dMSD(t)}{dt}$, self-diffusion coefficients (D) of gases in the PL were found from mean squared displacement as a function of time, $\mathrm{MSD}(t) = \langle [x_i(t) - x_i(0)]^2 \rangle$.

3.4 Results and Discussion

3.4.1 Structure and porosity. One concern when synthesizing PLs from porous organic cages is how robust the cages' porosity is. It is important to ensure that the pore that exists in the solid compound is maintained once dissolved into a liquid. Problems may arise if components of the liquid are able to invade the cavity, or if the cage is not rigid enough and collapses. In our proposed PL, although the Li^+ ions are small enough to enter the ACC pore, the complex of Li^+ and 12-crown-4 ether would be large enough to stay outside of the cage. Even so, investigation into the coordination of crown ether

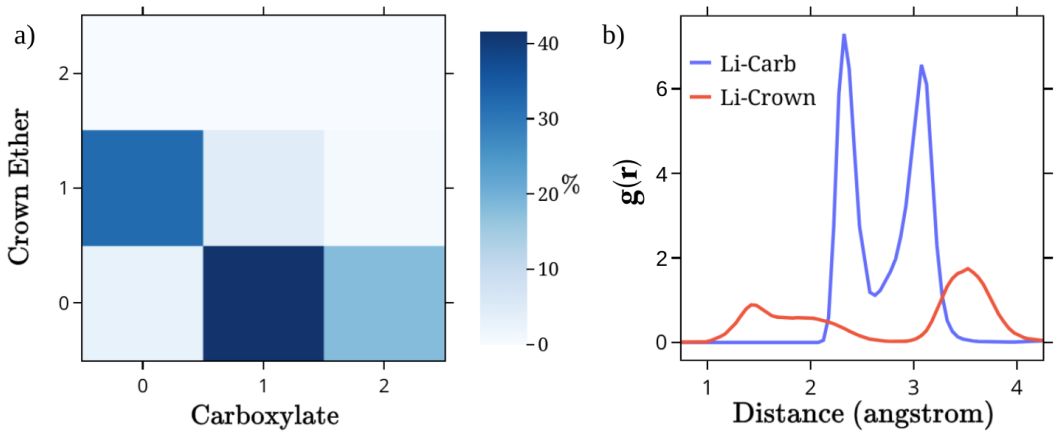

Figure 3.2 Li^+ coordination in ACC PL. a) Heatmap probability distribution of Li^+ coordination number to crown ethers and/or carboxylate groups within 4.0 Å. b) Radial distribution function of carboxylate (blue) and crown ether (red) around Li^+ ions.

around Li^+, shown in Figure 3.2a, suggested that Li^+ was only complexed to a crown ether ~35% of the time. However, the strong ionic interaction with the anionic groups on the outside of the cage keeps most non-complexed Li^+ within 2.3 to 3.1 Å of a carboxylate group rather than inside the pore.

Further structural analysis of the neat PL revealed that the ACC remained largely empty upon dissolution into crown ether, illustrated in Figure 3.3a. There is a small exception shown in Figure 3.3b, presenting itself as a small shoulder between 1 and 2 Å. This arises from the rare occurrence in which a Li^+ ion makes its way into the ACC cavity, however, given the low probability of this occurring, we do not believe this will greatly affect porosity. As shown in the figure, there remains an abundance of pores large enough to house single or multiple gas molecules, with an average pore diameter of 4.25 Å. This pore diameter is larger than the kinetic diameters of CO_2, N_2, and CH_4, of 3.47, 3.58, and 4.05 Å, respectively, as indicated by the dashed lines in the figure.[10]

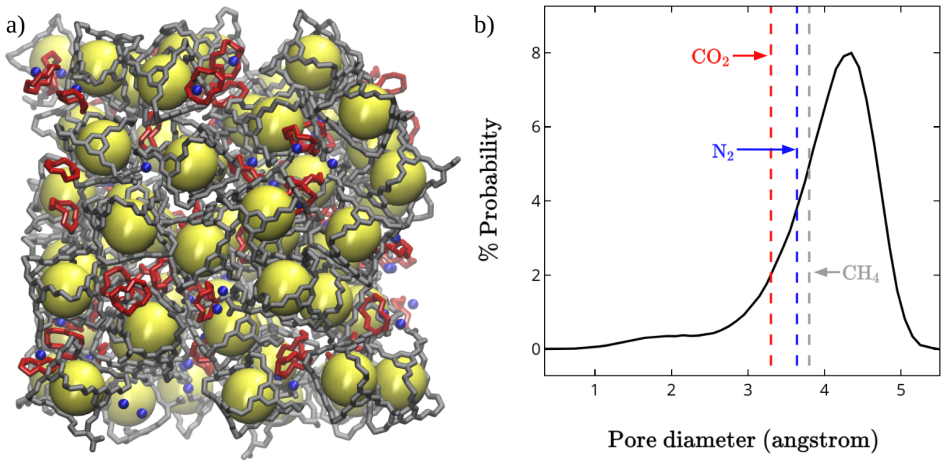

Figure 3.3 Porosity of ACC PL. a) Snapshot of equilibrated simulation box containing 64 ACC (grey), 64 12-crown-4 ether (red), and 64 Li^+ (blue), and permanent pores highlighted as yellow spheres. b) Pore size distribution of ACC PL, with kinetic diameters of CO_2 (red), CH_4 (grey), and N_2 (blue) marked as dashed lines.

In describing the shape of the dissolved ACC, which resembles an octahedron in the gas phase optimizations, we used a descriptor to compare the cages' rigidity in the neat ACC PL and when gases are also present. The descriptor calculated is defined as the distance between two opposite "vertices" of the cage, each vertex being the central C-C bond along each linker, as drawn in Figure 3.4. This measure can be thought of as how stretched or compressed an ACC molecule is, depending on if the distance is longer or shorter, respectively. Figure 3.4 shows the probability distribution of this descriptor and how it varies upon gas absorption. When CO_2 is included in the simulation, there is a downshift of the average distance, though the shape of the distribution is mostly consistent with the neat liquid. The most notable deviation from the neat PL, is when CH_4 is added, and there appear to be two major conformations of ACC, one compressed and one stretched. We suspect that this distortion is related to the fast movement of gas molecules through the cages, outlined later in mean squared displacement and cage occupation lifetime analyses.

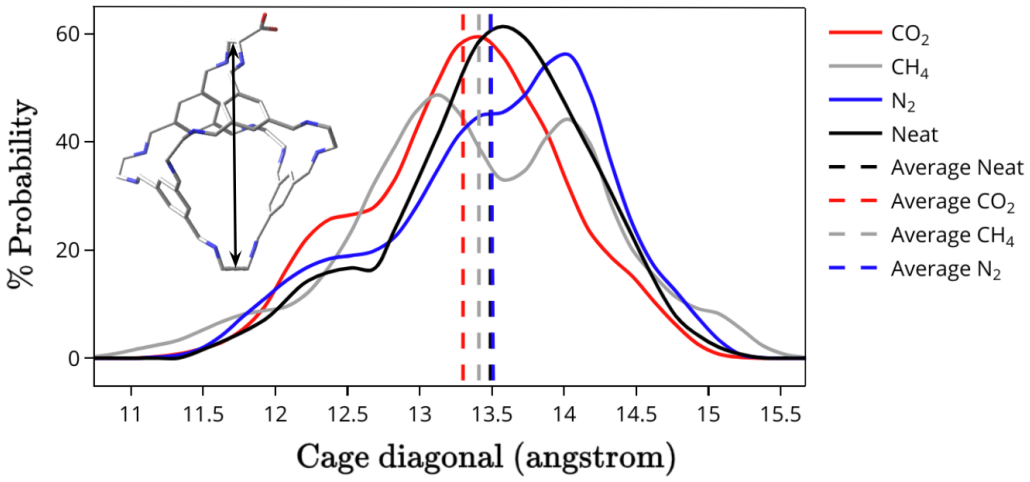

Figure 3.4 Effect of gases on ACC rigidity. Probability distribution of the cage diagonal (drawn in the upper right corner) in the neat ACC PL (black), and with CO_2 (red), CH_4 (grey), and N_2 (blue) dissolved in the PL. Average cage diagonals shown as dashed lines.

3.4.2 Gas-cage interaction. When gas molecules are introduced into the PL, we see that the large majority occupy the ACC central cavities or windows. Here we define occupation as any time the gas molecule's center of mass is within 5 Å of the geometric center of an ACC. As shown in Table 3.1, both CH_4 and N_2 remain in one ACC cavity for an average of ~400 ps. In contrast, the average CO_2 molecule will stay in the same ACC for over 12 ns, more than 30 times longer than the other gases simulated. This suggests that there is some strong interaction between CO_2 and the pore of the cage, or that there is a larger energy barrier to overcome for CO_2 to leave. Despite the contrasting average occupation lifetimes, all of the gases simulated had comparable probabilities for occupying ACC at any given point in the simulation, ranging from 86.62% to 92.51%. This means that CH_4 and N_2 are able to very quickly move in and out of a cage, and perhaps move on to a neighboring cage, suggesting that a network of pores exists in the PL.

Table 3.1 Lifetime analysis of gases occupying ACC.

Gas	% of Time Occupying ACC	Average Occupation Lifetime (ps)
CO_2	92.51 %	12759.5
CH_4	86.62 %	391.5
N_2	89.64 %	399.7

Beyond the binary of a gas molecule being either “in” or “out” of a cage, we wanted to know very specifically where within the cage the gas tended to be. Figure 3.5a shows the radial distribution function (RDF), g(r), of the gas molecule center-of-mass around the center of an ACC molecule in our PL simulations. We can see that while all three gases have a peak at 0 Å, indicating a prevalence of gas molecules at the very center of the cage, CO_2 also has a couple of secondary peaks around the 1 and 2 Å points. This suggests that CO_2 will actually spend significantly more time than the other gases in or near the windows of the cage, which is likely due to the greater length of CO_2. Despite a seemingly lesser affinity for the direct center of the ACC pore, CO_2 still spends more time within the core 2.8 Å boundary of the cage molecule when compared to CH_4 and N_2, as shown by the integral of g(r) in Figure 3.5a.

For a three-dimensional representation of the RDF, we calculated spatial distribution functions (SDFs) to show high-density areas for gases to be in and around a cage molecule, illustrated in Figure 3.4c-e. We postulate that in a perfectly symmetric cage, the SDF of gas within the cage would be symmetric as well, like the one drawn in Figure 3.5b. ACC, having an anionic group on one end, is not symmetric, which is why the different gases seem to prefer different ends or windows of the cage in relation to the anionic group. For all three, there is a noticeable difference in density between the two windows closest to the anionic group, and the two windows further away from the anionic group. CO_2 and N_2 seem to prefer the farther windows, and CH_4 prefers the closer windows. Understanding how gases respond to different functional groups may serve in further design and tunability of cage molecules for gas separation purposes.

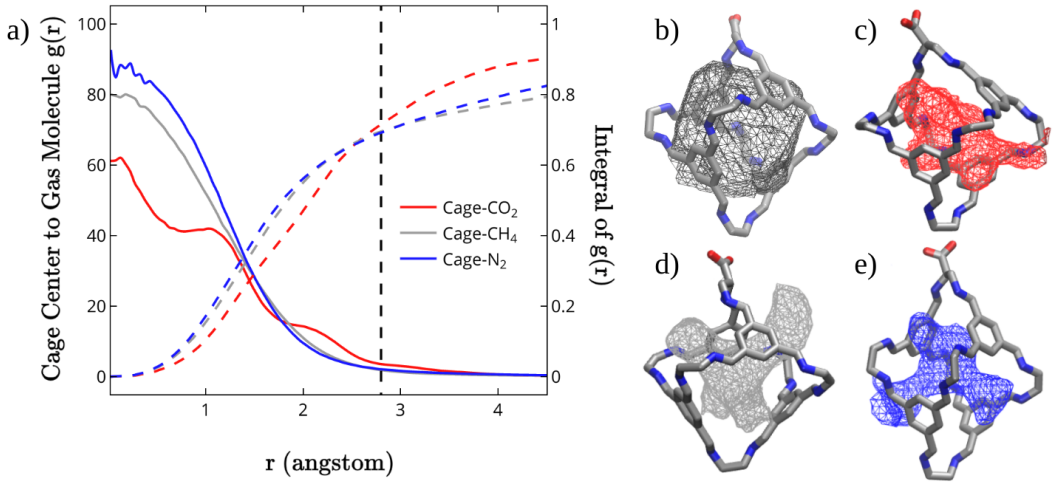

Figure 3.5 Gas placement within the cage in ACC PL. a) Radial distribution function, g(r), (solid) and integral of g(r) (dashed) of a gas molecule center-of-mass around the geometric center of an ACC molecule. CO_2 shown in red, CH_4 in grey, and N_2 in blue. Black dashed line indicates ACC core boundaries. b) Unoccupied pore space in neat ACC PL. High-probability areas for c) CO_2, d) CH_4, and e) N_2 to occupy the cage in the PL.

3.4.3 Thermodynamics. Solubility is an important measure in determining how effective a material is as a gas separation or carbon capture medium. In Figure 3.6a, we compare the GCMC predicted solubilities of each gas in ACC PL with simulated adsorption isotherms with Langmuir fitting. We can see that for CO_2 more milligrams of gas is absorbed per gram of PL compared to the other gases, especially at pressures between 1 and 2 bars. From the isotherms, we also calculated the isosteric heats of absorption, *q*st, for each gas as a function of amount absorbed, shown in Figure 3.6b. For all gases, the q_{st} decreases as more gas is absorbed, but CO_2 has the highest q_{st} overall, indicating that it is more thermodynamically favorable for CO_2 to be absorbed into the PL.

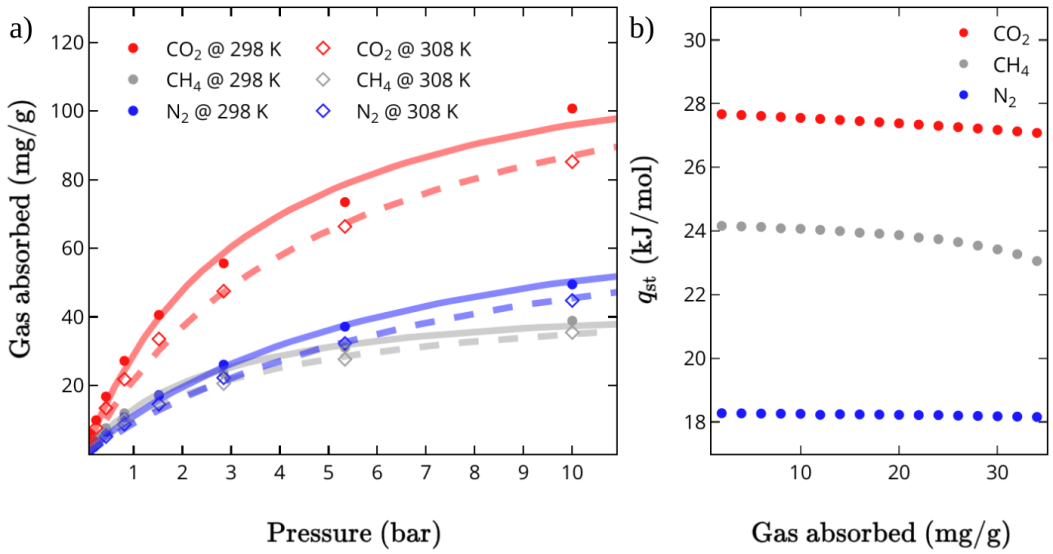

Figure 3.6 Solubility and absorption. a) Adsorption isotherms of CO_2 (red), CH_4 (grey), and N_2 (blue) in ACC PL at 298 K (solid circles) and 308 K (hollow diamonds). Langmuir fits are drawn for 298 K (solid lines) and 308 K (dashed lines). b) Isosteric heats of absorption (q_{st}) for CO_2 (red), CH_4 (grey), and N_2 (blue) as a function of gas absorbed.

3.4.4 Gas capture energetics. With umbrella sampling, we mapped the free energy change as a gas molecule leaves an ACC molecule in the PL, drawn in Figure 3.7. The core and branch boundaries are drawn at 2.8 Å and 5.0 Å, respectively, which are regions where we expect energetic barriers to arise, as the gas molecules leave areas of porosity. The energetic barrier for CO_2 leaving at the branch boundary line is about double that of CH_4 and N_2 molecules leaving an ACC, confining the CO_2 inside the cage as shown in the lifetime analysis earlier in Table 3.1. This free energy difference is low enough, though, that absorbed CO_2 could readily be removed with heat and the PL regenerated.

Paired with solubility, diffusivity of a solute provides helpful information regarding the gas permeability of a material. We calculated the mean squared displacement over time of the gases moving through the PL, as shown in Figure 3.8, and

applied the Einstein relation to predict self-diffusion constants, *D*, listed in Table 3.2. The extremely low diffusivity for CO_2 can be explained by looking back on the longer occupation lifetime that CO_2 experiences compared to CH_4 and N_2. Although CH_4 and N_2 had similar average occupation lifetimes, the faster diffusion by N_2 may be thermodynamically driven, due to the smaller heat of absorption for N_2.

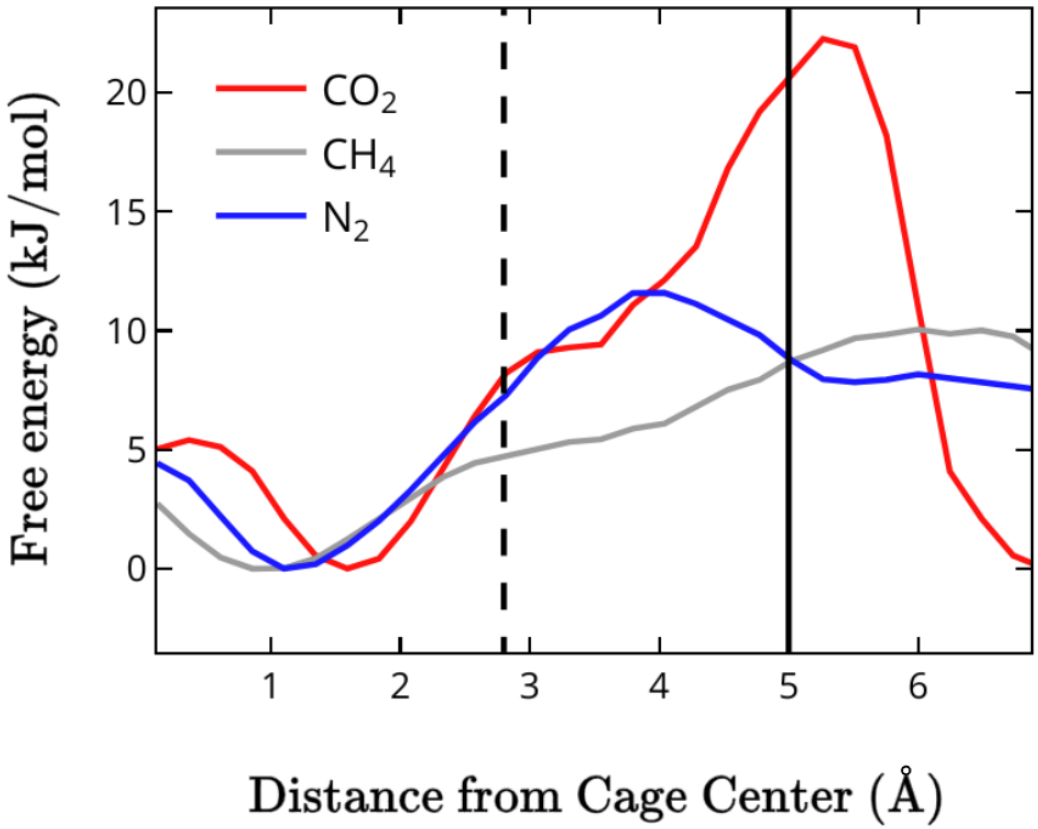

Figure 3.7 Gas capture energetics. PMF of CO_2 (red), CH_4 (grey), and N_2 (blue) exiting an ACC molecule. Black lines indicate boundaries of ACC core (dashed) and branch (solid) regions.

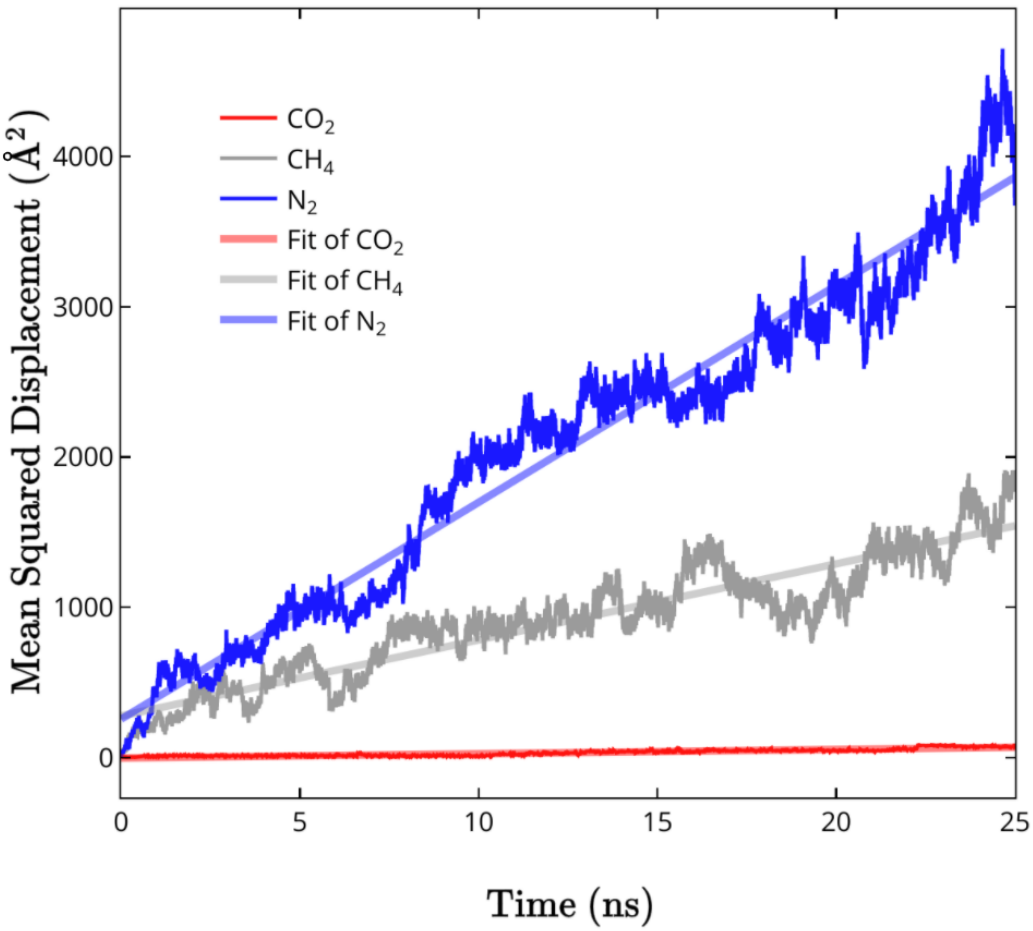

Figure 3.8 Self-diffusion in ACC PL. Mean squared displacement of CO_2 (red), CH_4 (grey), and N_2 (blue) in ACC PL over time.

Table 3.2 Gas self-diffusion constants, *D*, derived from Einstein's relation.

Adsorbate	*D* (cm^2/s)
CO_2	4.750×10^{-8}
CH_4	8.435×10^{-7}
N_2	2.405×10^{-6}

3.5 Conclusions

Along with other computational methods, we performed classical molecular dynamics simulations of a novel PL and assessed its performance as a gas separation material. Our results show that upon dissolution, the ACC pore remained intact and that a majority of the pores were large enough to house one or more small gas molecules. The gases tested included CO_2, CH_4, and N_2, and our analyses suggest a high favorability for ACC PL to trap CO_2 molecules within the ACC pores. This is in part due to a kinetic process, where a CO_2 molecule remains inside a single ACC more than 30 times longer than CH_4 or N_2. CO_2 was also found to have a higher solubility than the other gases in the PL, especially between 1 and 2 bars of pressure. Thermodynamically, CO_2 showed energetic favorability with greater isosteric heats of absorption compared to the other gases tested. While CO_2 had a higher solubility, the self-diffusion constant of CO_2 through the PL was orders of magnitude lower than those of CH_4 and N_2, as CO_2 was better contained within the large ACC molecule.

Our computational results show that the proposed ACC PL may serve as an effective fluid porous material for CO_2/N_2 separations or CO_2/CH_4 separations. Further studies looking at mixtures of these gases would be needed to directly address this point, however our findings show a clear affinity for CO_2 uptake over the other gases. Because of the modular design of the porous organic cage compound, cages with different substitutions can easily be designed and synthesized. It would be advantageous to understand how these variations affect gas-cage interactions and separation properties, and if the compounds could be precisely tuned for certain applications. As our work

suggests, the carboxylate group appears to have some effect on gas entry and exit paths, so other functional groups may have similar or varied effects.

3.6 References

1. Scholl, D.S.; Lively, R.P. Seven chemical separations to change the world. *Nature* **2016**, *532*, 435–437.

2. Schrag, D.P. Preparing to Capture Carbon. *Science,* **2007**, *315*, 812.

3. Aaron, D.; Tsouris, C. Separation of CO_2 from Flue Gas: A Review. *Sep. Sci. Technol.* **2005**, *40*, 321−348.

4. Schott, J.A.; Do-Thanh, C.L.; Mahurin, S.M.; Tian, Z.; Onishi, N.C.; Jiang, D.E.; Dai, S. Supported bicyclic amidine ionic liquids as a potential CO_2/N_2 separation medium. *J. Membr. Sci.* **2018**, *565*, 203-212.

5. Lee, J.; Kim, J.; Hyeon, T. Recent progress in the synthesis of porous carbon materials. *Adv. Mater.* **2006**, *18*, 2073–2094.

6. Long, J.R.; Yaghi, O.M. The pervasive chemistry of metal-organic frameworks. *Chem. Soc. Rev.* **2009**, *38*, 1213–1214.

7. Eddaoudi, M.; Kim, J.; Rosi, N.; et al. Systematic design of pore size and functionality in isoreticular MOFs and their application in methane storage. *Science* **2002**, *295*, 469–472.

8. Diercks, C.S.; Yaghi, O.M. The atom the molecule, and the covalent organic framework. *Science* **2017**, *355*, 1585.

9. O'Reilly, N.; Giri, N.; James, S.L. Porous liquids. *Chem. Eur. J.* **2007**, *13*, 3020–3025.

10. Mehio, N.; Dai, S.; Jiang, D.E. Quantum Mechanical Basis for Kinetic Diameters of Small Gaseous Molecules. *J. Phys. Chem. A*, **2014,** *118*, 1150.

11. Frisch, M.J.; Trucks, G.W.; Schlegel, H.B.; Scuseria, G.E.; Robb, M.A.; Cheeseman, J.R.; Scalmani, G.; Barone, V.; Petersson, G.A.; Nakatsuji, H.; et al. **2016**, Guassian 09, Gaussian, Inc., Wallingford, CT.

12. Wang, J.; Wolf, R.M.; Caldwell, J.W.; Kollman, P.A.; Case, D.A. Development and Testing of a General Amber Force Field. *J. Comput. Chem.*, **2004**, *25*, 1157.

13. Martínez, L.; Andrade, R.; Birgin, E.G.; Martínez, J.M. Packmol: A Package for Building Initial Configurations for Molecular Dynamics Simulations. *J. Comput. Chem.* **2009**, *30*, 2157.

14. Case, D.A.; Betz, R.M.; Cerutti, D.S.; Cheatham, T.E., III; Darden, T.A.; Duke, R.E.; Giese, T.J.; Gohlke, H.; Goetz, A.W.; Homeyer, N.; et al. **2016**, AMBER 2016, University of California, San Francisco.

15. Dassault Systèmes BIOVIA, Materials Studio 5.0, San Diego: Dassault Systèmes, **2017**.

16. Kumar, S.; Rosenburg, J.M.; Bouzida, D.; Swendsen, R.H.; Kollman, P.A. THE weighted histogram analysis method for free‐energy calculations on biomolecules. I. The method. *J. Comput. Chem.* **1992**, *13* (8), 1011-1021.

17. Mehio, N.; Dai, S.; Jiang, D.E. Quantum Mechanical Basis for Kinetic Diameters of Small Gaseous Molecules. *J. Phys. Chem. A*, **2014,** *118*, 1150.

CHAPTER FOUR

Conclusions & Future Work

4.1 Conclusions

The overarching aim of this work is to use computational methods to design novel materials for separations, predicting key properties, with the goal in mind of eventually synthesizing and testing these materials in the real world. Reaching this goal requires an understanding of the methods involved, ensuring that they reliably translate with experimental results, comparing simulated data to experimental. Once this is done, we can reasonably predict how new materials might be effective in separations, even before they have been created in a lab. Beyond that, computation opens deeper insights into how molecules behave on the atomic level, which can further our understanding of sorbate-sorbent interactions, and how they contribute to the larger picture.

Approaching this goal, we began with a previously synthesized ionic liquid (IL). Though ILs have been extensively studied in both simulation and experiment, this IL was unique in that it presented a polyethylene glycol-linked dication. [DBU-PEG][Tf_2N]$_2$ was first introduced as the solvent component in a type 3 porous liquid (PL), which paired the IL with ZIF-8.[1] We studied the properties of [DBU-PEG][Tf_2N]$_2$ as a neat liquid, as well as when CO_2 is absorbed into the bulk IL, using classical molecular dynamics (CMD) methods. We found that the simulations reproduced experimental density, viscosity, and x-ray diffraction (XRD) spectra.

Determining that this model was appropriate for further study, we looked further into the structure of the neat IL, and learned that the dication had two major conformations in the simulation: an "extended" configuration, where the two cationic centers were more separated, about 9.25 Å apart, and a "compressed" one, in which the cationic centers were much closer together with 7.30 Å of separation. We found that the PEG linker contributed to a weakened ionic interaction by separating the cationic and anionic centers. Structural information that is especially relevant to gas separation media is porosity and free volume, as these empty spaces may house small gas molecules. Because this IL has no permanent pores, we represent this measure as a cavity distribution, essentially showing how large an average empty cavity can be in the simulation box. This showed an average pore diameter of about 2.70 Å, which is smaller than the kinetic diameter of CO_2 (3.47 Å), however, a large amount of pores still exist beyond that threshold.

We then introduced CO_2 into the system to study the gas-liquid interactions. We found that the charge distribution and shape of the dication allowed for a distinct relationship with the gas, wherein a CO_2 molecule coordinates along the PEG linker and a CO_2 oxygen with a DBU group. The combined contributions of the geminal design and the bicyclic-amidine groups for the cation inspire the potential for similar dications, perhaps with longer or varied linking groups, and for an analogous dianion design in future works. Considering the IL's previous use in a PL, it is also worth studying further the role this IL plays in the PL, and its potential for other PLs or membrane materials.

The next part of this work focused on a cage-based porous ionic liquid, made up of anionic covalent cages (ACC) and lithium-12-crown-4 ether complex counterions. The cage component of the ACC PL has a single carboxylate group, lending the cage its anionic charge. The cage itself has four windows to access a central cavity about 4.25 Å in diameter, which is a suitable size for one to three small gas molecules like CO_2, N_2, and CH_4, thus making this PL a potential gas separation material.[2] In this work, we used CMD to study the structure and dynamics of both the neat PL and the liquid with different gases absorbed, paying close attention to the gas-cage interactions and energetics associated with such interactions. We also performed grand canonical Monte Carlo (GCMC) calculations to predict adsorption isotherms and heats of adsorption for each of the gases being absorbed by the PL.

Simulations of the neat PL found that the cage maintained porosity with an average pore diameter of 4.25 Å, ensuring that the Li^+ and crown ether molecules did not invade the ACC. In introducing the three gases into the system, we see that all were absorbed by the ACC, with CH_4 molecules existing inside the cage 86.6% of the simulation time, N_2 molecules inside for 89.6% of the time, and CO_2 92.5% of the time. The length of time that any one molecule stayed inside the same cage, however, was drastically different between gases. For CH_4 and N_2, the average time of stay was just under 400 ps, but when a CO_2 molecule entered an ACC pore, it stayed for an average of about 12.8 ns, over 30 times longer than the other small gas molecules. This means that CH_4 and N_2 interact with ACC with quick entries and exits, while CO_2 stays inside the

cage for longer periods, perhaps due to an energetic barrier to exit or favorable interactions with the inside of the cage.

Taking a look at where, not just when, a gas exists inside the ACC, we found that while CH_4 and N_2 molecules tend towards the geometric center of the cage, CO_2 molecules are commonly in the center and also nearer to the windows of the cage. From the GCMC calculations, we predicted the solubility of each gas in the PL, noting that CO_2 had the highest solubility per gram of PL, particularly at pressures between 1 and 2 bars. From these isotherms, we also determined the isosteric heats of absorption (q_{st}) for each gas, finding that CO_2 had the highest q_{st} of about 27 kJ/mol at 30 mg gas absorbed per gram of liquid. The q_{st} of CH_4 at the same amount of gas absorbed is about 23 kJ/mol, and the q_{st} of N_2 is just over 18 kJ/mol. CO_2 is therefore the most thermodynamically favored of the three gases.

We calculated the free energy change as the gas molecules entered and exited an ACC with umbrella sampling methods. This showed that at the outer bounds of the cage, between 3 to 5 Å from the geometric center, there is a larger energetic barrier of 22 kJ/mol for CO_2 to overcome in order to leave the cage. In contrast, N_2 must overcome a barrier of about 12 kJ/mol and CH_4 only 10 kJ/mol. The larger energetic barrier for CO_2 supports our earlier theory explaining the longer time of stay CO_2 experiences as a result of energetics. We also studied the diffusivity of the gas molecules over the course of the simulations by calculating the mean squared displacement over time, and determined the self-diffusion constants, *D,* for each gas. We found that N_2 was the most mobile with a *D* of 2.405×10^{-6} cm^2/s, followed by CH_4 at 8.435×10^{-7} cm^2/s, and CO_2 the least mobile

with D equal to 4.750×10^{-8} cm^2/s. The much lower D value for CO_2 results from how long CO_2 stays inside the largely stationary ACC.

4.2 Future Works

As stated above, this work aims at designing and studying tunable materials for separations, specifically liquids for carbon capture. The IL we studied in the first part of this work, [DBU-PEG][Tf_2N]$_2$, while previously used in a PL, may also be of interest for those studying membranes for gas separation.[1] This could be done both experimentally and computationally, with simulations confining the liquid between two-dimensional sheets as a supported ionic liquid membrane (SILM).[3,4] [DBU-PEG][Tf_2N]$_2$ had also combined the benefits of bicyclic-amidine groups tethered by a linker in a geminal design, a concept that could be further explored with other cationic groups and other linkers.[5,6] Similarly, applying an analogous approach to a dianion in an IL is worth looking into, especially given the great role the anion is known to play in ILs for gas separations.[7]

While our results are encouraging in showing the ACC PL's preference for CO_2 over the other gases simulated, in order to more accurately model how the PL would work in real-world applications, simulations of the PL with a mixture of gases would be necessary. In a similar vein, one might wonder how the PL would perform in other chemical separations.[8,9] The pore size is large enough to house monatomic ions, like xenon or krypton, and selecting for one over the other with low energetic cost would be valuable. In the case of the ACC PL, the modular design of the cage component lends

itself to be easily modified.[10] There are endless possibilities of similar cages featuring different substituting groups, whether charged or neutral, the number of those groups per cage, and the counterions or solvents to be paired with the cages. Of course, with such numerous potential PL designs, it would be crucial to understand how these variations affect the PLs efficacy as a separation medium. By doing so, one could reasonably tune a PL for precise purposes based off of these design criteria.

4.3 References

1. Shan, W.; Fulvio, P.F.; Kong, L.; Schott, J.A.; Do-Thanh, C.L.; Tian, T.; Hu, X.; Mahurin, S.M.; Xing, H.; Dai, S. New Class of Type III Porous Liquids: A Promising Platform for Rational Adjustment of Gas Sorption Behavior. *ACS Appl. Mater. Interfaces* **2018,** *10*, 32.

2. Jie, K.; Onishi, N.; Schott, J.A.; Popovs, I.; Jiang, D.E.; Mahurin, S.; Dai, D. Transforming porous organic cages into porous ionic liquids via a supramolecular complexation strategy. *Angew. Chem. Int. Ed.* **2020,** *59,* 2268-2272.

3. Hanioka, S.; Maruyama, T.; Sotani, T.; Teramoto, M.; Matsuyama, H.; Nakashima, K.; Hanaki, M.; Kubota, F.; Goto, M. CO_2 separation facilitated by task-specific ionic liquids using a supported liquid membrane. *J. Membr. Sci.* **2008,** *314,* 1-4.

4. Budhathoki, S.; Shah, J.K.; Maginn, E.J.; Molecular simulation study of the performance of supported ionic liquid phase materials for the separation of carbon dioxide from methane and hydrogen. *Ind. Eng. Chem. Res.* **2017,** *56,* 6775-6784.

5. Schott, J.A.; Do-Thanh, C.L.; Mahurin, S.M.; Tian, Z.; Onishi, N.C.; Jiang, D.E.; Dai, S. Supported bicyclic amidine ionic liquids as a potential CO_2/N_2 separation medium. *J. Membr. Sci.* **2018**, *565*, 203-212.

6. Bara, J.E.; Hatakeyama, E.S.; Gabriel, C.J.; Zeng, X.; Lessmann, S.; Gin, D.L.; Noble, R.D. Synthesis and Light Gas Separations in Cross-Linked Gemini Room Temperature Ionic Liquid Polymer Membranes. *J. Membr. Sci.* **2008,** *316,* 186.

7. Liu, H.J.; Dai, S.; Jiang, D.E. Molecular dynamics simulation of anion effect on solubility, diffusivity, and permeability of carbon dioxide in ionic liquids. *Ind. Eng. Chem. Res.* **2014,** *53,* 10485-10490.

8. Kewley, A.; Stephenson, A.; Chen, L.; Briggs, M.E.; Hasell, T.; Cooper, A.I. Porous organic cages for gas chromatography separations. *Chem. Mater.* **2015,** *27,* 3207-3210.

9. Miklitz, M.; Jiang, S.; Clowes, R.; Briggs, M.E.; Cooper, A.I.; Jelfs, K. Computational screening of porous organics molecules for xenon/krypton separation. *J. Phys. Chem. C* **2017,** *121,* 15211-15222.

10. Hasell, T.; Cooper, A.I. Porous organic cages: soluble, modular, and molecular pores. *Nat. Rev. Mater.* **2016,** *1,* 16053.